Design of Energy Storage System for Motorsports Based on the Statistical Analysis of the Mission Profile

Undergraduate Honors Thesis

Presented in Partial Fulfillment of the Requirements for Graduation with

Honors Research Distinction in the Department of Mechanical Engineering at

The Ohio State University

By

Yatin Khanna

Undergraduate Honors Program in Mechanical Engineering

The Ohio State University

2020

Thesis Committee:

Dr. Giorgio Rizzoni, Advisor

Dr. Matilde D'Arpino, Co-Advisor

Prof. Yann Guezennec

Abstract

Motorsports has been the proving ground for novel automotive technology since the last century; hence it is fitting territory to research and develop the next generation of electric powertrains. The backbone of any electric vehicle is the energy storage system, and this research thesis aims to streamline the development process of energy storage systems for electric race vehicles competing in any electric motorsports category by statistically evaluating the mission profile.

The technical and sporting regulations define the mission profile for any racing category, and it provides a reasonable estimate for the power and energy demands to compete and win the race successfully. By studying the regulations and analyzing the power profiles of the race vehicles from six different racing events, a handful of statistical metrics are established to evaluate the battery specifications in terms of charge and discharge rate of the battery pack.

Using the established metrics, a generalized methodology is developed to assess the charge and discharge current rate requirements, and the output of the metrics is used to select the most appropriate and lightweight cell chemistry. Battery pack sizing is performed on the chosen cell chemistry to determine the battery cell used to develop the lightest battery pack as lowering the weight is one of the highest priorities in racing applications. A Heat generation analysis is performed at pack level using a zero-order cell model. The outcome is the battery pack's analytical design with the most fitting cell chemistry and estimated heat generated for a given mission profile.

Dedication

Dedicated to my parents and my sister, Shashi and Tilak Khanna, and Yashika for all their sacrifices to help me follow my passions and live my dreams

Acknowledgments

I would like to thank my advisor Dr. Giorgio Rizzoni for giving me the opportunity to pursue undergraduate research at the Center for Automotive Research and his guidance throughout the process. I am grateful to my co-advisor, Dr. Matilde D'Arpino, for being the inspiring figure she is. I feel incredibly fortunate to have the opportunity to work with her on this research project. Her constant guidance and support made the research a joyous learning experience. I would also like to thank Prashanth Ramesh for his valued feedback in developing the research methodology and teaching me about batteries. I will cherish those lessons for life.

I am thankful for the valued feedback from Prof. Yann Guezennec as the thesis committee member. His insightful assessment helped in improving the thesis outcome.

Last but not least, I am grateful to have a supportive family in India and express deep gratitude to Barkha and Madhur Sharma, my aunt and uncle, for giving me a family away from home. I would not be where I am without the constant love and support from my family. I am also grateful to have a friend like Kritagya Arora, who is always there in my lows and highs.

Vita

September 10, 1997 …….. Born – Gurugram, Haryana, India

December 13, 2020 …….. B.S. Mechanical Engineering, The Ohio State University, Columbus, Ohio

Table of Contents

List of Tables

List of Figures

Chapter 1: Introduction to Motorsports

1.1 History of Motorsports:

At the dawn of a sunny day in August of 1888, [1] Bertha Benz took to the road to become the first motorist to drive from Mannheim to Pforzheim in her husband's invention, the "Benz Patent-Motorwagen" and changed human history. Not long after her [2] 180-kilometer trip, the automotive enthusiasts turned to racing in the streets. Almost seven years later, [3] in 1895, the first truly organized racing event was held in France. The pilots traversed 1,178 km to drive back and forth between Paris to Bordeaux. The racing enthusiasts began organizing events across the pond in the US with the [3] 87 km race between Chicago and Evanston in Illinois on the thanksgiving eve of 1895.

Figure 1. 1 Bertha and Carl Benz driving the Motorwagen [1]

The thrill-seekers spread the racing bug across Europe and North America. Governing bodies such as Automobile Club de France (1895) formed to define the rules and regulations in

Europe. By 1900, the cars became almost thrice as fast as it was in 1895, and [3] achieved speeds more than 80.96km/h. The governing bodies and the racers took racing to purpose-built tracks with the notable exception of "Mille Miglia." The cars competing in the races on both sides of the pond were usually the prototypes of the following year's models [3]. After World War 1, the racing teams started building purpose-built cars with specialized seats, fuel tanks, and tires to complete.

The first French Grand Prix held in 1906 and Indianapolis 500 in 1911 opened the flood gates to various motorsports. Stock-car, hot-rod, and drag racing originated in the US and spread worldwide after world war 2. In Europe, Grand Prix racing and endurance racing gained popularity, with the events organized in France, Italy, Germany, and Monaco throughout the 1920s [3]. The races were governed by the Association Internationale des Automobiles Clubs Reconnus, renamed Fédération Internationale de l'Automobile or FIA in 1946. Until the 1950s, individual race events were held across Europe with a few disruptions because of world war 2. In 1950, the world championship for drivers was instituted by the FIA [3].

The FIA started defining the sporting and technical regulations for cars in 1946, and the premier racing category was named "Formula A." The word 'formula' refers to the regulations. The first race under the formula was held in Turing in 1946, won by Achille Varzi in the Alfa Romeo 158 Alfetta. The first race of the driver's championship was held at Silverstone, the UK, in 1950, and the first driver's title was won by Giuseppe ("Nino") Farina. One characteristic common across the motorsports categories was the internal combustion engine (ICE), albeit Andrew Riker was pioneering electric vehicles (EV) and won races while competing with the conventional ICE-powered cars. "Riker drove this automobile to victory in a race at Charles River Park near Boston in 1899 and another race in 1900 against a field of gasoline- and steam-powered vehicles." [5]

Electric cars started garnering the public's interest around the dawn of the 20th century and reached its heyday by the end of the first decade. A third of the vehicles on the US roads were electric until the Ford Model T was introduced. The cheaper gasoline-powered cars and fuel killed the EV by 1935 [5]. With no interest in EV, motorsports continued to develop the ICE to be more powerful and reliable. ICE started as a 0.75hp single cylinder [7] prime mover at the dawn of the 20th century, and by the dying years, ICE was pushing over 1000hp [8]. The electric propulsion was nowhere in sight until the FIA decided to introduce a "new road-relevant, energy-efficient power source" [9] in F1.

KERS or the kinetic energy recovery system allowed the driver to recuperate energy during braking and store in an energy story system (ESS), and deploy 80hp for 6.6 seconds over the course of a lap [9]. However, it would not be wrong to say that F1, the premier motorsports category was a little late to the electrification party. Formula lightning was a collegiate open-wheel formula-style race that traveled to the major racetracks around the US [10]. The cars were putting out 350 volts [11] from 31 lead-acid batteries [10], reaching speeds of 140mph. The Ohio State University team achieved the highest ever recorded 147mph [11] in 2000. The pit-stop included a change of batteries, which the team managed in 17 seconds [12].

1.2 Background and Motivation:

The electrification of F1 was followed in endurance racing and the development of road-worthy technologies to improve the mass-production cars [13]. Albeit electric racing came to the limelight with the formation of FIA Formula-E (FE) in 2013. The series aims to "demonstrate the potential of sustainable mobility to help create a better, cleaner world" [14]. Since the first race in 2014 at

Beijing Olympic Park, FE has grown to 12 teams with automotive giants Mercedes, BMW, Audi, Porsche, Nissan, Jaguar, DS, and Mahinda lining up the grid in the sixth season of FE. Venturi automobiles are another team on the FE grid with a history of popularizing EV. They have developed the world's fastest EV in collaboration with Ohio State, called the Buckeye Bullet 3, and the world's fastest electric motorcycle, Venturi Voxan Wattman.

With the rise in the popularity of EV [15] in the consumer market, automotive giants' focus is shifting towards electric motorsports. Mercedes and Porsche joined the FE grid for the 2019-2020 season, while BMW receded from open-wheel racing categories in 2009 entered the 2018-2019 FE season. Volkswagen developed the ID. R to obliterate the track records around the globe [16]. The renewed interest of automotive manufacturers in open-wheel racing indicates the development potential that motorsports offer for road cars. As Jaguar's FE team principal said, "The reality is there are real translations in the technology from Formula E to our future production cars" [17]. The FE rules are designed to force the team to focus their resources on developing the road-relevant powertrain rather than working on the aerodynamics and chassis [18].

The motorsport series's technical regulations define the kind of technological development required for the sport. Formula 1 is a constructor series, which means every team needs to develop their chassis and bodywork, albeit the teams can buy powertrain from a common engine manufacturer [19]. Formula E falls between one-make series and constructor series; chassis, bodywork, and battery are common for all teams, developed and manufactured by common manufacturers [20]. Teams can develop their powertrain or buy it from another team [20]. FIA and FIM technical regulations for electric land-speed racing provide guidelines for the battery pack, chassis, bodywork specifications, and homologation [22, 23]. Hill climb racing such as Pikes-peak

and Isle of Man TT have lax regulations regarding the powertrain development compared to F1 or FE, albeit the governing body regulates the battery voltage and current limits.

It is essential to understand the sporting and technical regulations of various electric racing categories to determine the mission profile to develop the powertrain. This thesis will investigate the three different electric racing categories spread among six different events to develop a generalized optimal design methodology for battery cell selection based on the duty cycle and the governing regulations. Table 1 summarizes the racing events and vehicle specifications.

Racing Series	**Formula E**	**E-Kart**	**Buckeye Current (PPIHC)**	**Buckeye Current (IOMTT)**	**Voxan Wattman**	**VBB3** [4]
Weight (kg)	900	125	228	250	300	3175.15
Max Speed (km/h)	280	110	181.30	282.57	408	549.43
Race Duration (min)	46.5	15.5	11.05	17.37	≈2	≈2
Energy (kWh)	54	2.96	7.7	27	≈4.5	≈96
Power (kW)	250	30	217 / 405	127 / 153	≈200	2237
Voltage (V)	878	84	480	600	≈800	800
Battery weight (kg)	280	30	70.3	131	≈150	1600
Cooling system	Liquid	Forced-Air Cooling	Air-cooled	Passive / Thermal mass	Forced Air	Passive
Data source	Canopy Simulation	Test data from UNCAS	Buckeye Current	Buckeye Current	Race data by CAR	Simulation data by CAR
Resolution	Variable step size	0.0010	0.1	0.2	1	0.01

Table 1. 1 Summary of Racing Events and Vehicles

1.3 Thesis contribution

Even though the motorsport categories such as Formula E were formulated to develop road-worthy technologies, there is a substantial difference in the development process of electric road-legal cars and electric race cars. The gargantuan differentiator is the end-product usage; road cars are designed with cost and efficiency at the focal point, whereas race cars are designed with the passion and zeal for speed, requiring an atypical approach to research and development. This thesis aims to provide such an unorthodox method for developing an energy storage system that can be generalized to all-electric motorsport categories to streamline and abate the process of conceptually designing the battery pack.

The duty cycle of an electric race vehicle is defined by the category's technical and sporting regulations. The magnitude of power that the vehicle can put down on track during the operation defines the power demand from the battery pack, i.e., the battery pack's power profile. The battery pack power profile can be estimated from the race simulations or the vehicle's telemetry data. The battery pack designed for the race vehicle is expected to suffice the power profile requirements, albeit there is a disengagement between the battery cells' datasheets and the power profile.

The power profile provides information about the power required at a given point in time, but it does not provide information about the expected discharge or charge rate of the battery pack, which is the paramount factor when choosing the right cell chemistry. It is also essential to know the duration, magnitude, and variability in charge and discharge current during the operation to design the lightest, and power and energy-dense energy storage system for racing application.

In the following sections, power profiles for multiple electric racing categories are statistically analyzed, and generalized metrics are defined, in an attempt to co-relate the battery power profiles with the battery pack specifications. Followed by the application of the defined generalized metrics to choose the right cell chemistry for a race vehicle, conceptual battery pack design, and heat generation analysis for the power profile.

Chapter 2: Introduction to Li-ion battery cells

2.1 History of Li-ion Cells

SONY marketed Li-ion batteries (LIB) in 1991 [1], followed by A&T Battery Co. in 1992 [2]. The LIB offers higher energy density compared to nickel-cadmium (Ni-Cd) or nickel-hydride (Ni-MH) batteries while not being subjected to the memory-effect in the latter chemistries [2]. The SONY LIB utilized lithium cobalt oxide (LCO) as the positive electrode and coke negative electrode [1] as LCO is relatively insensitive to production variability and moisture. Since the inception of LCO LIB, other chemistries such as $LiFePO_4$ (LFP), $LiMn2O_4$ (spinel), Li $(NiMnCo)O_2$, (NMC), and Li $(NiCoAl)O_2$ (NCA) have been introduced as the positive electrode substitute [1]. The various positive electrode chemistries offer different advantages such as high C-rate, thermal stability, long cycle life, high capacity, and low cost, allowing the manufacturers to choose chemistries (Table 2. 1) for specific applications [4].

Specification	$LiCoO_2$ (LCO)	$LiMn_2O_4$ (LMO)	$LiFePO_4$ (LFP)	$LiNiMnCoO_2$ (NMC)
Voltage (V)	3.60	3.80	3.30	3.60/3.70
Charge Limit (V)	4.20	4.20	3.60	4.20
Cycle Life	500-1000	500-1000	1000-2000	1000-2000
Specific energy (Wh/kg)	150-190	100-135	90-120	140-180
Specific power	1C	10C, 40C (Pulse)	35C continuous	10C
Safety	Average. Required protection circuit & cell balancing		Very safe, needs cell balancing & voltage protection	Safer than LCO. Needs cell balancing & voltage protection
Thermal Runaway	150°C	250°C	270°C	210°C

Table 2. 1 Characteristics of various commonly used LIB [4]

Even though the LIB was commercialized at the dawn of the '90s, the development started in the early '70s. Matsushita introduced lithium-carbon monofluoride (Li-CFx) primary cell in 1973, and in 1975 Sanyo introduced lithium-manganese dioxide primary cells (Li-MnO2) [2]. After the introduction of primary cells, the research was focused on the development of Li-ion secondary cells. Li metal as anode caused safety issues because of the formation of dendrites [2]. The safety issues prompted a shift to intercalation material such as graphite for the anode, first patented by H. Ikeda of Sanyo in 1981, a year later of Goodenough filing for LCO cathode patent [2]. Kuribayashi and A. Yoshino used LCO as cathode and graphite as the anode to develop the first safe to use LIB and patented it worldwide [2]. SONY used the same patent to commercialize its first LIB in 1991.

2.2 Working of Li-ion Cells

The four main components of a cell are the positive electrode and negative electrode, the electrolyte, the separator, and the collector. The negative electrode, in general, is a pure metal; for LIB, it is usually graphite [1], and the positive electrode material is commonly a metal oxide and lithiated metal phosphate for LIB [1]. The electrolyte is the pathway for ionic charge transfer between the electrodes. Cells with voltage lower than 2V use an aqueous ionic conductor electrolyte. Most of the LIB use nonaqueous ionic conductor electrolyte as the nominal voltage is much higher than 2V [3]. The separator is an electric insulator and an ion conductor; its primary purpose is to isolate the two electrodes and prevent internal short-circuiting [3]. The current collector serves as a junction between the active electrode material and the outside world. The active electrode material is adhered to the collector to form an electronic connection to the load. The collector does not take part in the chemical reaction inside the cell [3].

During the discharge process, the electrons are released into the external circuit, and positively charged ions are released into the electrolyte at the negative electrode due to the electrochemical potential energy [3]. The positive electrode accepts the electrons from the external circuit and the positive ions from the electrolyte [3]. This transfer of electrons and positive ions from the negative electrode to the positive electrode creates an electromotive force or cell voltage between the two electrodes [3]. During the charging process, an external electromotive force is applied to reverse the positive ions' motion and the electrons from the positive electrode to the negative electrode [3]. The positive electrode acts as an anode during the charging process, and the negative electrode serves as the cathode, but for this thesis, the electrodes are referred to as positive and negative depending on the active material. Table 2. 2 summarizes the behavior of the electrodes during charging and discharging.

Process	Negative Electrode	Positive Electrode
Discharging	• Gives up e^- to the external circuit. • Electrode is oxidized • Anode	• Accepts e^- from the external circuit. • Electrode is reduced • Cathode
Charging	• Accepts e^- from the external circuit. • Electrode is reduced • Cathode	• Gives up e^- to the external circuit. • Electrode is oxidized • Anode

Table 2. 2 The behavior of the electrodes during charging and discharging

LIB work in a slightly different manner than described in the previous paragraph. LIB is an insertion-electrode cell, also known as the rocking chair cell. In Figure 2. 1, the small red spheres are lithium, and the green and purple planes are the negative and positive electrode active material crystals, respectively [3]. The wall in between the two electrodes is the separator. Li exists as a neutral atom between the layers of the electrode crystals. Li atom is small enough to exist in the carbon lattice's interstitial sites without disturbing the crystal structure. During the discharge

process, Li in the negative electrode loses its loosely held valance electron to the external circuit, and the Li+ ion is ejected into the electrolyte (deintercalation), and it is absorbed by the positive electrode (intercalation) to become neutral by accepting the electron from the external circuit. The opposite happens during the charging process as the transfer process is entirely reversible. Due to the back and forth transfer of the Li between the electrodes, the LIB is called a rocking chair cell.

$$Li \Rightarrow Li^{+} + e^{-} \text{ (Negative electrode)}$$

$$Li^{+} + e^{-} - \Rightarrow Li \text{ (Positive electrode)}$$

Eq.1 Insertion-electrode mechanism in LIB [3]

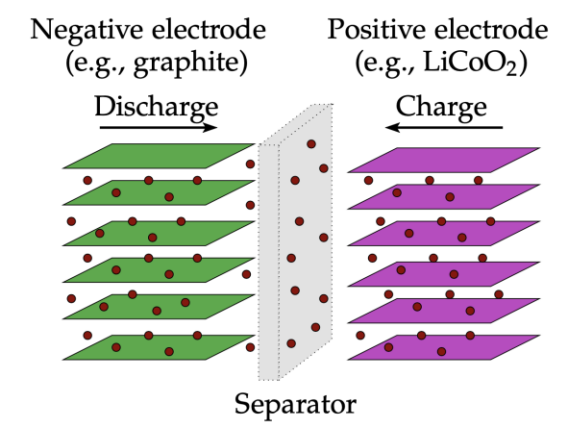

Figure 2. 1 Li-ion cells working mechanism

2.3 LIB chemistries and form factor

LIB are available in various form factors with a wide range of energy and power density. One of the biggest advantages of LIB over other chemistries is the higher specific energy (Wh/kg), specific power (W/kg), energy density (Wh/l), and power density (W/l), which helps in developing lighter and smaller packs essential for motorsports application. Figure 2. 2 shows the Ragone plot of energy storage devices; the LIB hold high specific energy while maintaining a comparatively

high specific power [4]. This characteristic of LIB translates into a long-range and high-accelerating vehicle necessary in all forms of EV racing. Figure 2. 3 shows the comparison of energy density and specific energy [5]. LIB have the highest energy density, and specific energy, which makes it perfect for motorsports application as smaller and lighter energy-dense battery packs can be developed to suit the volumetrically constrained lightweight powertrains.

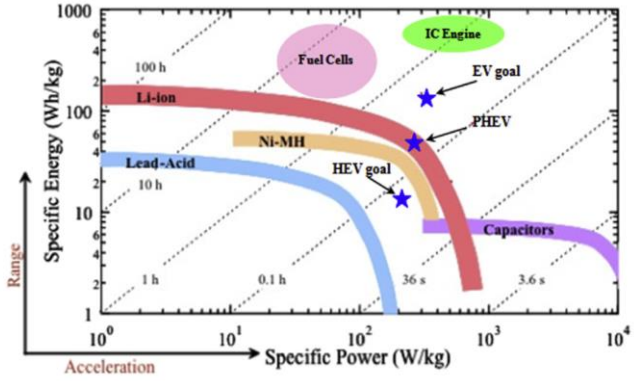

Figure 2. 2 Ragone plot [4]

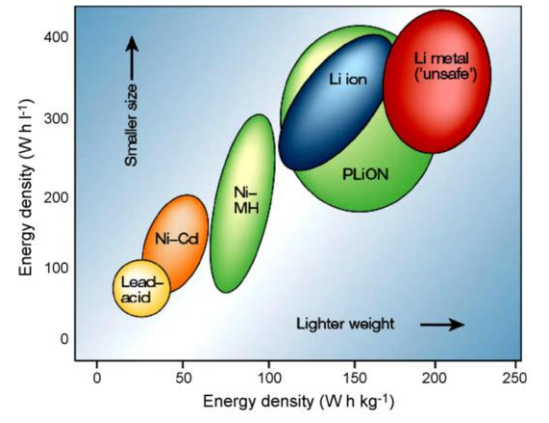

Figure 2. 3 Energy density vs. specific energy [5]

The wide range of LIB formats available in the market makes it the go-to chemistry for motorsports applications. Depending on the volumetric constraints, duty cycle, and the racing series's technical regulations, the most appropriate type of cell format can be adopted. Figure 4

shows the three most prominent types of LIB formats currently available. Cylindrical, prismatic, and pouch cells have their pros and cons, summarized in table Table 2. 3 [4].

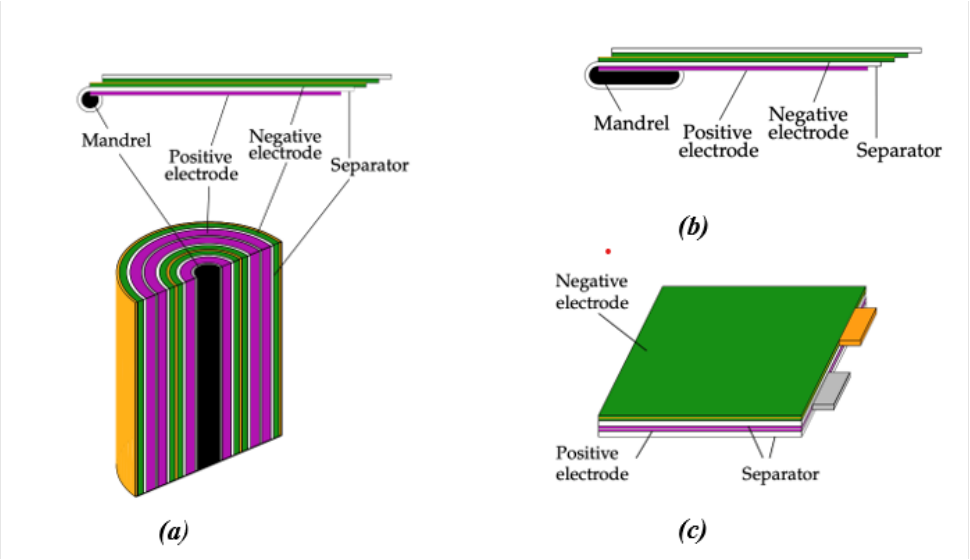

Figure 2. 4 . Schematic structures of LIB [3] (a.) Cylindrical cell (b.) Prismatic cell (c.) Pouch cell

The cylindrical cells are jelly-rolled around a cylindrical mandrel that becomes the cell's cell's positive terminal. In the prismatic cells, the thin sheet of active electrode material separated by the separator is wound around a flat mandrel giving it a prismatic appearance [3]. The jelly rolled cells are housed in a metal casing and filled with electrolyte. The pouch cells are made by stacking the active electrode material separated by the separator and housed in a soft aluminum pouch filled with electrolyte [4].

The cell's capacity is directly proportional to the active material area, and the heat dissipation depends on the heat exchange surface area per unit volume [4]. The higher the heat exchange surface area per unit volume higher the heat transfer from the cell and the lower the

internal temperature. For example, comparing a cylindrical (38120), prismatic (1865140), and pouch cell (W: 73.35 mm, H: 163.40 mm, T: 10.60 mm), the heat transfer areas per unit volume are about 105.26 m^{-1}, 156.17 $m^{-1,}$ and 228.19 m^{-1} respectively [4]. The pouch cell has the highest area per unit volume, which reduces the thermal resistance and makes it suitable for high C-rate applications as the internal temperature rise would be minimal. The better thermal performance of prismatic and pouch cells is offset by the additional weight added to the pack to maintain the compressive force on the electrode to maintain an even contact as lower quality [4].

Different manufacturers use different LIB cell geometry in the production cars. Tesla most famously uses over 7000 18650 cells for Model S. The benefits of using smaller cell are higher cost efficiency, lower thermal aging, and a higher level of safety albeit the increase in interconnection increase the number of failure point as well as the reduced weight and volume [4] efficiency could be an issue while developing the pack for racing purpose.

The choice of chemistry and geometry is highly dependent on the application. Some significant factors such as the volumetric constraints, weight, operating environment, and the vehicle's duty cycle play a significant role in choosing the cell chemistry. For a hypothetical race scenario of land speed racing in salt flats, the most suitable cell chemistry would be LNMC or LNCA from Figure 2. 5 because of high power density. A cylindrical or prismatic geometry offers high structural integrity at the cell level and would reduce the weight of the pack as less packaging material would be required to build a mechanically sound battery pack.

	Small Cylindrical	Large Cylindrical	Prismatic	Pouch
Shape	Contained in a metal casing	Contained in a metal casing	Contained in semi-hard plastic or metal casing	Contained in a soft aluminum bag
Connections	Welded nickel or copper strips or plate	Threaded stud for a nut or threaded hole for a bolt	Thread hole for a bolt	Tabs that are clamped, welded, or soldered
Retention against expansion	Inherent from the cylindrical shape	Inherent from the cylindrical shape	Requires retaining plates at ends of the battery	Requires retaining plates at ends of the battery
Appropriateness for small projects	Poor: high design effort, requires welding	Good: some design effort	Excellent: little design effort	Very poor: design effort too high
Appropriateness for production runs	Good: welded connections are reliable	Good	Excellent	Excellent
Field replacement	Not possible	Possible	Possible	Not Possible
Delamination	Not possible	Not possible	Possible	Highly possible
Compressive force holding	Excellent	Excellent	Poor	Extremely poor
Thermal management	Not favorable	Not favorable	Favorable	Favorable
Heat dissipation	Poor	Poor	Fair	Good
Local stresses	No	No	No	Yes
Safety	Good	Good	Good	Poor
Ease of assembly	Poor	Poor	Excellent	Poor
Heat shrink wrapping	Yes	Yes	Depend on casing	No

Table 2. 3 Comparison of cell formats

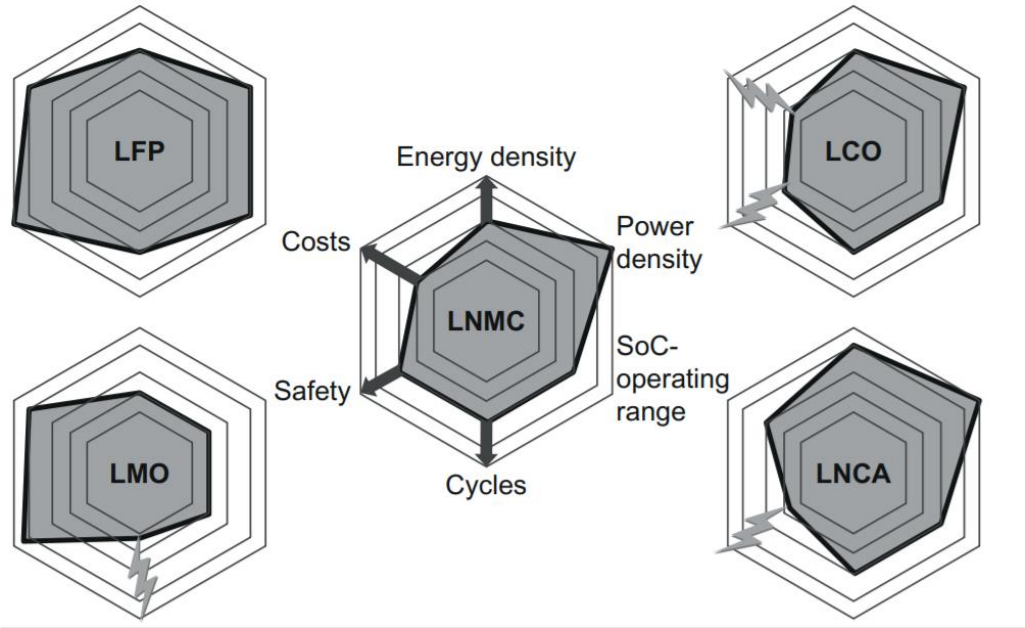

Figure 2. 5 Properties of Li-ion cell chemistries [6]

2.4 Thermal Management System Overview

LIB work the best around 23C; that is why it is essential to cool the LIB to maintain a constant working temperature or heat it to an appropriate working temperature. The battery thermal management (BTM) is the component of a LIB pack that performs the task of maintaining an optimal working temperature (10C - 40C) [7, 8]. In its most simple form, BTM is an integrated heat exchanger of some kind in the battery pack [7]. The integration of BTM in the battery pack depends on many factors, albeit it is important to understand the heat sources in the pack during its operation and the dependency on the external conditions and packaging of the pack.

LIB goes through an exothermic reaction during the discharge charge cycles and generates heat due to the high rate of reaction [7]. The LIB also incurs an increase in internal resistance with a change in the state of health, which increases the ohmic heating losses and adds up to the heat generated by the exothermic reaction [7]. The heat generated is also affected by coupled parameters such as electrochemistry, current, and heat transfer, which change with the state of charge (SOC), state of health, temperature, and duty cycle [9]. External factors such as the duty cycle, ambient temperature can also impact the heat generated in the cell. On the pack level, battery management system (BMS), cell balancing, and cell placement can act as proponents of heat transfer and increase the cell temperature.

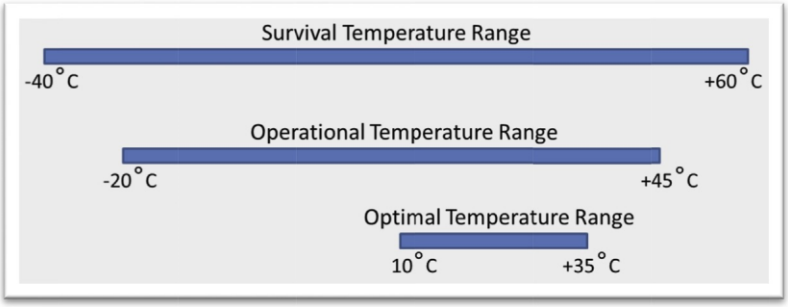

Figure 2. 6 Lithium-ion cell temperature ranges [1]

The optimal working range of LIB is between 10C and 40C, albeit it works between -20C and 50C, which is called the operational temperature range. Between -20C and -40C, the internal resistance of the cell increases as the electrolyte freezes, and above 60C, the cell chemistry becomes unstable; this range is called the survival temperature range. Figure 2. 6 visualizes all three temperature ranges [7]. Under all three temperature ranges, the cell is physically stable and safe to use. The user can run into safety issues once the LIB reaches thermal runaway temperatures. The thermal runaway temperature, like the working temperature range, depends on the chemistries of LIB. Table 2. 1 summarizes the thermal runaway temperature limits for different LIB chemistries [8].

The primary objectives of BTM are to keep the battery pack in the optimal temperature range and minimize the temperature gradient across the pack, which are achieved by either implementing active or passive cooling techniques. Forced/ram air induction, direct and indirect liquid cooling fall under the active cooling techniques. Application of phase change material and use of thermal mass fall under the passive cooling techniques. Cell arrangement at module and pack level also influences the effectiveness of the implemented cooling method. The cooling method and cell arrangement choice largely depend on the duty cycle and the cell geometry. The following sections will explore the most common active and passive cooling systems used in BEV.

2.4.1 Air-cooled

Air-cooled BTM is the simplest, cheapest, and lightest to implement in a vehicle [9]. Many Japanese and Chinese production BEV, such as BYD E6 and Nisan Leaf, use forced induction BTM driven by several fans. The simplicity and low price come at the expense of insufficient heat capacity and low thermal capacity. The heat transfer coefficient for an air-cooled system is dependent on the air mass flow, air temperature, cross-section of module/pack, cell spacing, cell geometry, thermal resistance, and flow path of the fluid. Factors such as air mass flow and air temperature depend on the induction system, which acts as a parasitic load. To increase the air mass flow and decrease the air temperature, energy from the battery pack would be consumed, reducing the vehicle's range.

The cross-section of the module/pack and flow path of the fluid depends on the cell geometry and spacing, which further depend on the cell's series and parallel arrangement to achieve the desired power and energy from the battery pack. A hypothetical battery pack with 2mm of cell spacing will have lower heat transfer between the cells than a pack with 1mm cell spacing, albeit the tight volumetric constraints of vehicles in motorsports might drive the design towards lower cell spacing. The heat transfer from the cells via convection also depends on the cell insulation's thermal resistance, thicker insulation around the cell might decrease the heat transfer but increase the cell temperature.

The flow path of the fluid directs the thermal gradient across the pack. It is vital to minimize the thermal gradient as the cells that routinely face higher temperatures would foresee a decrease in cell capacity and an increase in internal resistance, hampering the performance of the whole

pack [9]. Various cell arrangements for air-induction are shown in Figure 2. 7. The red color signifies a higher temperature, and the blue color, a lower temperature.

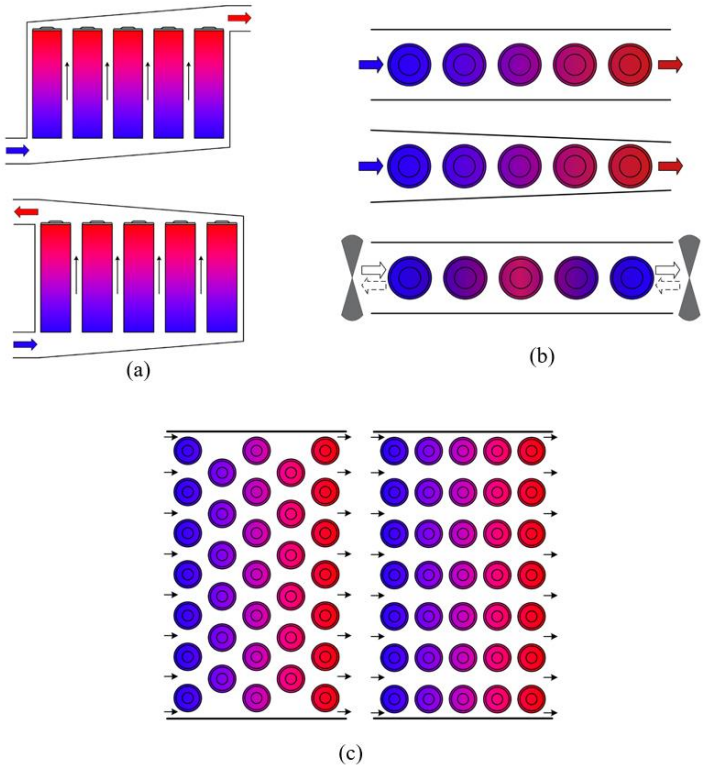

Figure 2. 7 Air cooling configuration (a) Parallel (b) Series (c) Series-parallel [3]

The parallel arrangement is the best option for limiting the thermal gradient across the battery pack, but it will require a much complex cooling circuit as compared to a series arrangement in which the air enters from one end and leaves from the other. Both the series and parallel configurations would result in battery packs with low volumetric efficiency, most of the production vehicles use the series-parallel combination (Figure 2. 7c), which is not the best alternative to achieve a small thermal gradient, but it is much more efficient in packaging as compared to series or parallel arrangement. The hexagonal arrangement's flow path in Figure 2.

7c is longer than the aligned configuration, which creates a larger thermal gradient, but the volumetric efficiency of the pack increases, increasing the energy and power density of the pack.

Ram air cooling can be substituted with active cooling using fans to reduce the parasitic loads as the race vehicle would always be in motion. The downside of ram air cooling is the drag penalty, as bigger openings in the bodywork would be needed to match the airflow from a forced-induction system. The simplistic nature of the air-cooled BTM system comes with its disadvantages, summarized in Table 2. 4. It might not be the ideal system for extended duty cycles, but it could be the best option for a shorter duty cycle if the cell temperature does not exceed the survival temperature range.

Pros	Cons
Cheap to implement	Low thermal conductivity
Lightweight	High parasitic power consumption
Least Complex	Creates thermal gradient
	Dependance on external environment conditions

Table 2. 4 Pros and cons of air-cooled BTM

2.4.2 Liquid-cooled

The liquid-cooled BTM system is similar to the air-cooled system in configuration, albeit with a much higher heat transfer coefficient and a much lower thermal gradient across the pack. Water/glycol or mineral oils are used for the liquid cooling system, further categorized into direct and indirect liquid cooling shown in Figure 2. 8. A metal plate with inbuilt cooling channels for the coolant sandwiches the battery cell at the face with the highest surface area to form the indirect liquid-cooled BTM [11]. In direct liquid-cooled BTM, the coolant, usually mineral oil, flows directly over the battery cell, cooling the faces with the highest surface area.

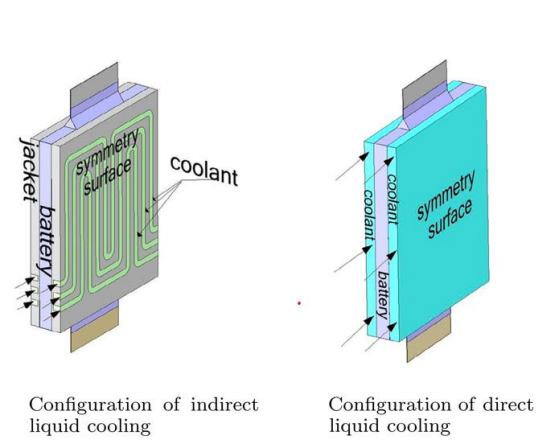

Figure 2. 8 Liquid cooling configurations for prismatic cell [5]

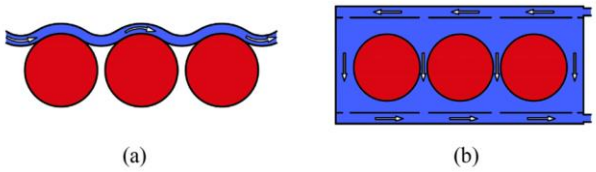

Figure 2. 9 Liquid cooling configurations for cylindrical cell (a) Direct (b) Indirect [6]

The liquid cooling system is much more complicated and heavier than the air-cooled system as a complex cooling network is required to circulate the coolant across the battery pack. The cooling circuity also adds multiple failure points, which could be catastrophic for a race vehicle. Though, the higher thermal conductivity can outweigh the added complexity and weight for a longer duty cycle. The thermal conductivity of water/glycol and mineral oil is 0.39W/mK and 0.13W/mK, respectively, an order of magnitude higher than the thermal conductivity of air, 0.0242W/mK. For longer duty cycles such as FE, it is necessary to keep the battery in optimal temperature range, and liquid cooling could be the best option.

The efficiency of liquid cooling highly depends on the geometry of the cell. A higher contact patch area is available for prismatic cells compared to the cylindrical cells in Figure 2. 9a. The smaller contact patch will reduce the heat transfer via conduction, reducing the system's

overall efficiency. Hence it is vital to do heat generation analysis to estimate the power to weight ratio for opting for the most appropriate cooling solution. The pros and cons of liquid-cooled BTM are summarized in Table 2. 5:

Pros	Cons
Higher thermal conductivity	Higher weight
Smaller thermal gradient	More complex
Lower parasitic power consumption	Potential of leakage and electric short
Compact as compared to air cooling system	Expensive and difficult to implement

Table 2. 5 Pros and cons of liquid-cooled BTM

2.4.3 Passive

Passive BTM is the simplest of the three cooling systems mentioned to implement. It uses either the battery pack's thermal mass to contain the generated heat or the latent heat of a phase change material (PCM) to remove the heat from the cells. The simplicity comes at a price of higher thermal gradients and an uncontrollable cooling system. The thermal mass of the battery pack can contain a specific amount of heat generated before the temperature of the battery pack exceeds the operations temperature range. The PCM can start melting during repetitive duty cycles, which reduces the heat transfer coefficient and increases the temperature of the battery pack. The PCM also adds more weight compared to an air-cooled system, which would decrease the specific power and specific energy of the battery pack. For short duty cycles, the thermal mass could be an effective solution if the cells remain in the operational temperature range throughout the duty cycle.

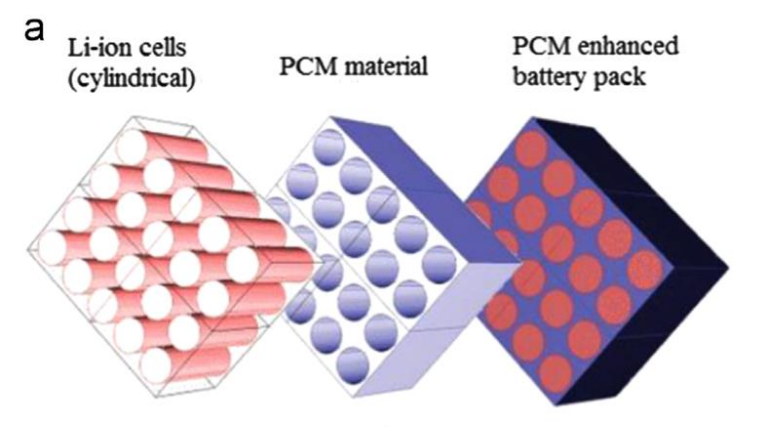

Figure 2. 10 PCM application

2.5 Comparing BTM solutions:

Two important factors to consider while selecting the cooling solutions are the additional weight and the duty cycle duration. A race vehicle must have high power to weight ratio. For higher acceleration and max speed, a colling system with more than the required cooling capability will slow down the vehicle because of additional weight. A longer duty cycle will result in a higher generation, which would require a BTM with high thermal conductivity. A balance between the additional weight and cooling capacity is necessary to optimize the battery pack for a specific application. Table 2. 6 provides a summary of BTM solutions material properties. Water/glycol offers higher thermal conductivity with the highest density, whereas forced air is the lightest with the lowest density. Mineral oil for direct liquid cooling is lighter than water/glycol, with a lower thermal conductivity, but the cooling system would require a much higher volume of mineral oil as compared to water/glycol as the battery pack would be completely flooded with it (Figure 2. 9b). PCM has the highest thermal conductivity, but all the free space in the battery pack will be filled with it (Figure 2. 10), increasing the overall pack's weight.

Property	Air	Mineral oil	Water/Glycol	PCM
Density (kg/m^3)	1.225	924.1	1069	866
Specific heat capacity	1006	1370	3323	1980
Thermal conductivity (W/mK)	0.0242	0.15	0.3892	16.6

Table 2. 6 Properties of BTM elements [6]

Assuming a constant average temperature rise while discharge of 35Ah (169mm X 179mm X 14mm) prismatic cell in Figure 2. 8, water/glycol mixture used for indirect liquid cooling consumes the least amount of power due to highest thermal conductivity out of the three materials compared in Table 2. 7:

	Air	**Mineral oil**	**Water/glycol**
Average temperature rise (°C)	8.4	8.2	8.3
Flow velocity V (m/s)	4	0.00275	0.015
Pressure drop (Pa)	148	279	189
Mass flow rate (g/s)	0.96	0.49	0.29
Ideal power consumption (mW)	116	0.15	0.051
Extra mass (kg)	Negligible	0.0298	0.0723
Mass percentage (%)	0	2.95	7.16

Table 2. 7 Design parameters of different cooling methods with same temperature rise [5]

The additional weight added to achieve the lowest power consumption is the highest for water/glycol due to the highest density. The power consumption for forced air cooling is the highest, but there is no weight penalty. The BTM solution for a battery pack, designed for a specific duty cycle, can combine the aforementioned solutions or one of the solutions. Formula E cars have the longest duty cycle, and it uses an indirect liquid cooling BTM, whereas the Voxan Wattman, which has the shortest duty cycle uses a combination of forced air induction and passive BTM using thermal mass. To choose the most efficient and lightweight BTM solution, it is vital to estimate heat generation during the duty cycle and predict the operational temperature range for the given battery pack.

Chapter 3 Definition of the case studies

3.1 Battery pack design for motorsports:

As mentioned in the previous chapter, the cell selection for a vehicle depends on multiple factors. The cell selection criteria for motorsports are also very different than the criteria for the automotive industry. The priorities are different because of the different end goals of the product.

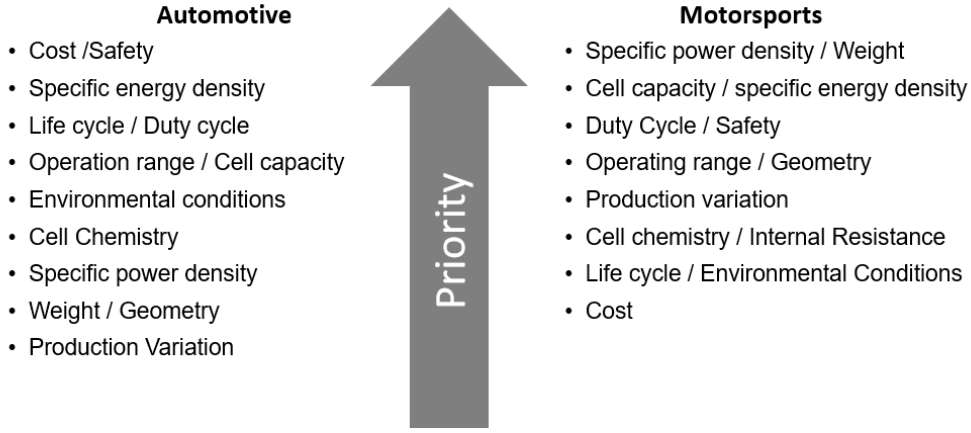

Figure 3. 1 Comparing cell selection criteria for motorsports and automotive industry

The cell selection criteria for automotive applications and motorsports applications are mentioned in Figure 3. 1.

1. The cost and safety are essential for both the automotive manufacturers and the motorsports teams, albeit both factors take a back seat when it comes to cell selection for race vehicles, as the priority is to make race vehicle fast.
2. The driving range for both the applications is critical; it is one of the factors that drive up the car sales and win a race the vehicles need to finish the race. The duty cycle and

cycle life is much shorter for racing application as compared to the battery electric vehicles (BEV) for road usage; the battery cells are pushed to the extreme edge to extract every bit of performance, which reduces the cycle life and the battery pack for motorsports application is not expected to last over a season or an event, hence it is not a crucial factor.

3. The push to the extreme edge makes production variation between the cells a crucial factor, as a cell with a capacity lower than nominal capacity could hamper the overall pack's performance.
4. As described in previous sections, different cell chemistries serve different purposes; if the race duration is longer, one would need to compromise the specific power for specific energy to gain the extra range.
5. Race vehicles tend to operate in extreme thermal operating windows; the chosen chemistry that suffices the specific energy and power criteria should work in intended conditions. The working conditions for a BEV are not that extreme as passenger vehicles' large size provides ample space to implement an active thermal management system to keep the temperatures under 50°C.
6. The cell's internal resistance depends on the chemistry of electrodes, and lower internal resistance at higher monetary cost could be the way to go for motorsports, but the marginal gains in thermal performance would not suffice the cost criteria for the automotive industry.
7. The cell geometry and weight are also crucial for motorsports as the packaging is tight to improve the vehicle's aerodynamic performance and rolling resistance, whereas the larger size of passenger vehicles makes cell geometry less critical.

The battery cell selection for motorsport events is further dependent on the event's mission profile, which is further divided into sub-categories, such as open-wheel racing, time-trial, land speed racing, DTM (Deutsche Tourenwagen Masters), and off-road racing. The end goal of all the categories is to make a fast race vehicle, but the duty cycle can vary. FE and E-kart racing fall under the open-wheel racing category, in which the driver goes around a closed race-track. DTM also follows a similar suit, albeit electric DTM cars are still in development and will not race until 2022. Time-trial racing requires the vehicle to be driven as fast as possible across a road course or hill-climb; the duty cycle is shorter than FE, but it is aperiodic as the length of straights and corners might not be the same across the course as compared to the closed race track for FE offering a redundant duty-cycle for every lap.

Off-road racing or Extreme-E series is still in the development phase; the race would be a rally-Esque race across extreme climatic conditions to test the durability of LIB and powertrain and motor. The priority of cell-selection for such an event would be highly dependent on the cell chemistry's thermal behavior, albeit not a lot of data about the duty cycle is available as of now. Land-speed racing is the most distinct of all as it requires the powertrain to put out an exponentially high amount of power compared to any other racing series in the shortest duration to maximize the vehicle's speed. Such a powertrain will require high specific power and energy to achieve the necessary speed and not run out of energy. The open-wheel racing, time-trial, and land-speed racing are further discussed in the following sections by exploring the technical regulations that define the mission profile and statistically evaluating the defined power profiles to choose the right cell chemistry.

3.2 Open-wheel race

Open-wheel race cars have the wheels and suspension outside the car's body, and any bodywork does not cover it. Formula E is the pinnacle of electric open-wheel racing, and the E-kart is the steppingstone into four-wheel racing. The races take place on closed circuits, where the driver complete n-laps depending on the race event and category. The duty cycle is periodic as the driver drivers around the same track layout multiple times. Formula E often races on street tracks, built by closing the streets of major cities such as Paris and New York, whereas the E-kart race around purpose-built go-kart tracks.

3.2.1 Formula E (FE):

The Formula E event comprises of three main events that take place in one day. Two practice sessions, one qualifying session, and the race event. During the practice session, the drivers and the teams learn about the track and car setup, the qualifying session sets the grid for the race event. During the race event, all the drivers compete on the track while driving around the track for a fixed amount of time. FE car specifications are summarized in Table 3. 1.

Figure 3. 2 Gen 2 Formula E Car

Qualification session:

1. The session is 1 hour long, and drivers are divided into four groups of max six depending on their championship position. Each driver is given six minutes to set the best-time lap.
2. The six fastest drivers move onto the super pole shoot-out, the fastest of the six starts in the front, and the rest according to their fastest lap-time. The drivers can use 250kW of power throughout the session.

Race:

1. The race is 45 min long and an additional lap.
2. The drivers can use 200kW of power throughout the session. The driver can gain an additional 35kW for a few laps by using the Attack Mode by passing through a slower racing line at the designated corner and 25kW from the fan boost.

Racing Series	**Formula E**
Weight (kg)	900
Max Speed (km/h)	280
Race Duration (min)	45min + 1lap
Battery Pack Energy (kWh)	54
Battery Pack Power (kW)	250 (Qualifying) / 200 (race)
Battery Pack Voltage (V)	878
Battery Pack Weight (kg)	280
Specific Power (W/kg)	~893
Specific Energy (Wh/kg)	~193
Cooling system	Liquid

Table 3. 1 Specifications of Formula E car

For the analysis, Marrakech E-Prix simulation data from Canopy Simulations Limited, UK, is used to analyze the FE's mission profile. The simulation is not correlated and validated with the trackside data, albeit it provides a reasonable estimation of the duty cycle. The mission profile will

vary from race to race, depending on the circuit layout, but the maximum power deployed and recuperated will remain the same. The objective of the analysis is to understand the power and energy requirement to choose a satisfactory cell-chemistry and thermal management system for the vehicle.

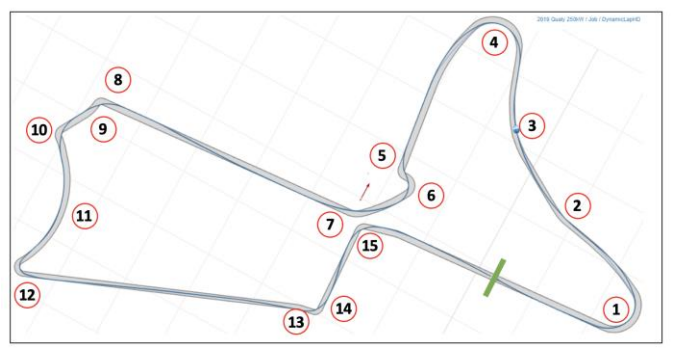

Figure 3. 3 Marrakech E-Prix track layout and racing line [20]

Figure 3. 3 is the layout of the 2.94km long counterclockwise Marrakech E-Prix track located in western Morocco's major economic center with 15 corners and three straights. The green line is the start/finish line, and the faint blue line across the track is the racing line used for the analysis. The racing line is the fastest way across the track, albeit it depends on the race conditions as well. The race and qualifying averages from season 5 and simulation in Table 3. 2 are numerically quite close, indicating that the simulation is a good estimator of the FE car's real-life performance.

Session	Data	**Season 5**	**Simulation**
Qualifying	Average Speed [km/h]	138.91	133.15
	Pace [s]	77.489	79.230
Race	Average Speed [km/h]	126.56	123.36
	Pace [s]	84.600	84.452

Table 3. 2 Comparing simulation averages and season 5 average

The data provided by Canopy Simulations consists of 11 race laps at varied average speeds and energy consumption. During the race, the driver needs to adjust the balance between power deployment and regeneration to optimize energy consumption to complete the race. For the analysis, 11 race laps are joined randomly to create a race simulation assuming the driver does not use the fan boost or attack mode. The simulation also assumes that the car is always moving during the race, i.e., pit stops and race starts are ignored.

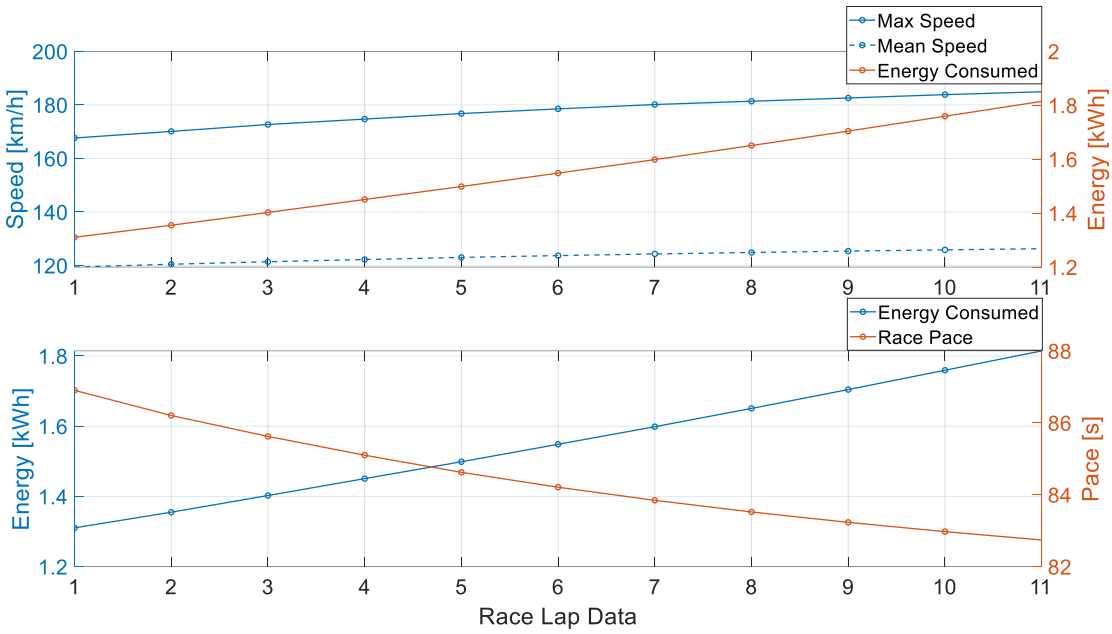

Figure 3. 4 Summary of 11 race lap profiles

The difference between 11 race profiles is visualized in Figure 3. 4. As energy consumption increases, the maximum speed increases, and the race pace decreases. If the driver dives at the 11th race lap profile consuming 1.81kWh per lap, they would need 60kWh of energy to complete the race; the battery pack is limited to 54kWh. Hence, they would have to shift between the race profiles to maintain the required race pace and save enough energy to complete the race.

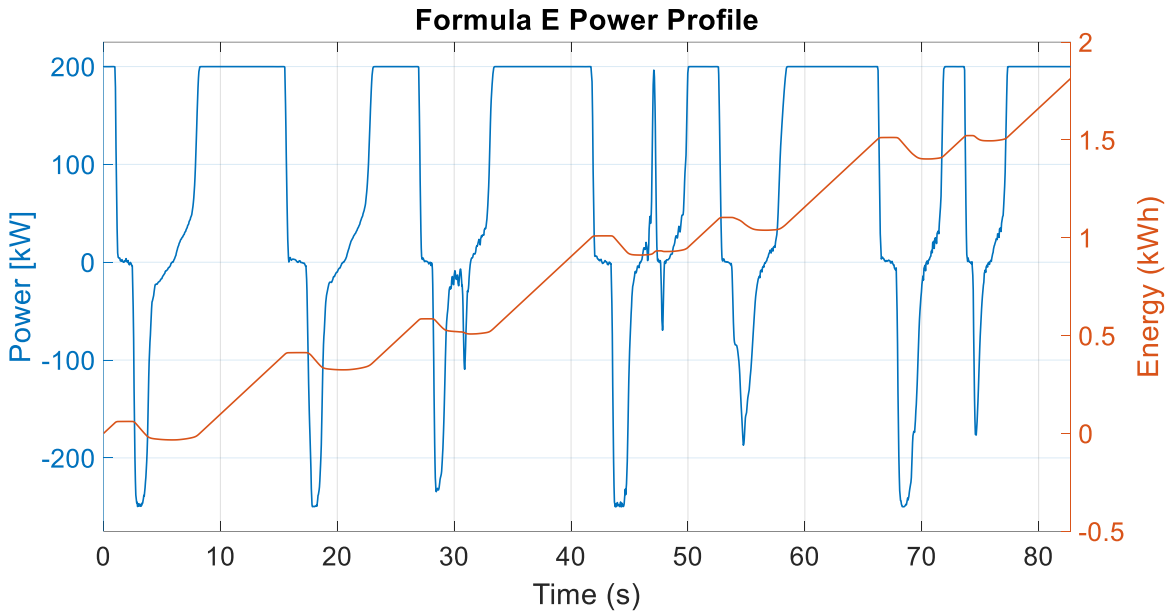

Figure 3. 5 Formula E power and energy profile

FE power profile plotted in Figure 3. 5 represents the power deployment (+ve Y-axis), regeneration (-ve Y-axis), and energy consumed during one lap. For most of the lap, the power deployed is constant at 200kW, and the slope of the energy vs. time plot is positive, indicating energy consumption. The power recuperation is much more variable than power deployment, and the slope of energy vs. time plot is negative, indicating energy regeneration. If there is no regeneration, then the energy vs. time plot will be a straight line. A similar power profile is repeated 33 times during the race, with the difference being the pulse duration for power deployment and amplitude and duration of regeneration pulse.

Figure 3. 6 is the visualization of Figure 3. 5 in Figure 3. 3, the blue part of the racing line represents power deployment, and the orange part is regeneration. The concentric red dot is the start-finish line with car cars driving in a counterclockwise direction. The energy recuperation happens between the start of braking until the middle of the corner when the driver applies power

to accelerate. The nine power deployment pulses in Figure 3. 5 represent the nine blue sections of the racing line, starting with the start/finish point and first braking point. The same trend follows for power regeneration pulses.

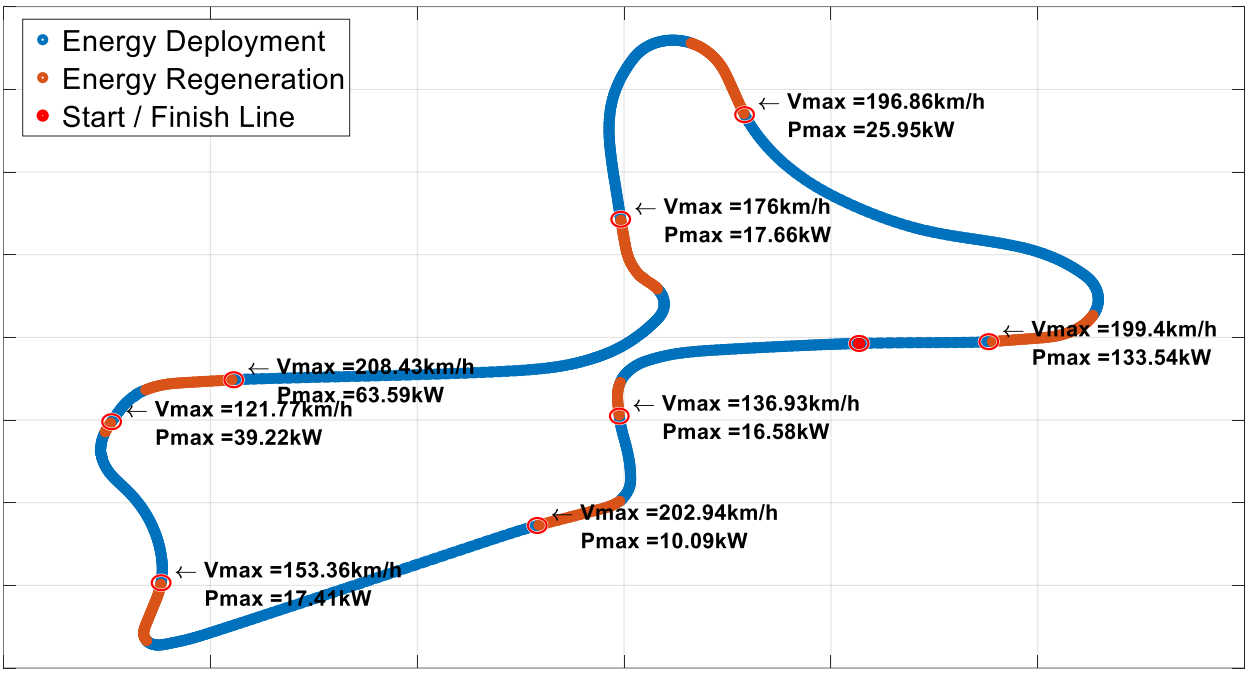

Figure 3. 6 Visualizing power profile on the racing line

The difference between the different race lap profiles is the length of the blue and orange sections, for race profile one in Figure 3. 4 consuming 1.3kWh energy, the blue sections will be shorter, and the orange sections will be longer as compared to profile eleven with 1.8kWh energy consumption.

3.2.2 -Kart:

Karting is the steppingstone to any form of four-wheeled motorsports. Traditionally the go-karts used in the CIK-FIA Karting World Championship are powered by the traditional ICE. The electric

karts or E-karts were introduced under the FIA's electric and new energy initiative to promote green mobility [21]. The E-kart analyzed is a 30hp E-kart developed by the University of Cassino and Southern Lazio G-Side Racing Team in Italy. The karts are designed according to 2015 - FIA Technical Regulations (Category V – Class 1) but are not homologated by the FIA.

Figure 3. 7 30hp E-kart developed by G-Side Racing Team

The kart is tested at a local go-kart track, almost 25km away from the University of Cassino, by traditional go-kart drivers. The E-kart is capable of energy recuperation, albeit it is ignored for this analysis because of the driver's driving style. While driving the go-karts with an internal combustion engine, the driver presses both the accelerator and brakes while entering a corner to keep the engine speed high enough to accelerate out of the corner; the E-kart is driven with a similar driving style, minimizing any opportunity for energy regeneration. The track is 1.1 km long, and the layout in Figure 3. 8 consists of 11 corners with an average lap time of 54.73s and an average speed of 63.37km/h. The kart's theoretical max speed is 110 km/h; on track, it achieves a max speed of 96.20km/h. The kart specifications are summarized in Table 3. 3.

Racing Series	30 hp E-Kart
Weight (kg)	125
Max Speed (km/h)	110
Race Duration (min)	~16
Battery Pack Energy (kWh)	2.96
Battery Pack Power (kW)	22
Battery Pack Voltage (V)	84
Battery weight (kg)	30
Specific Power (W/kg)	1000
Specific Density (Wh/kg)	99
Cooling system	Forced-Air Cooling

Table 3. 3 Specifications of 30hp E-kart

It takes an average of 0.16kWh of battery pack energy to complete the counterclockwise lap. The kart can complete approximately 17-19 laps in 15-17 minutes before running out of energy. The red circles in Figure 3. 8 represent the braking and the acceleration points, with the break in the pit-straight representing the start-finish line. The data shared by the G-side race-team consists of 14 lap profiles, similar to the FE data with slightly variant lap-times and energy consumptions. The data is acquired during the test sessions and is a good representative of race conditions. As aforementioned, regeneration is ignored to create a simulated profile by randomly concatenating the data to simulate a 17-lap race simulation.

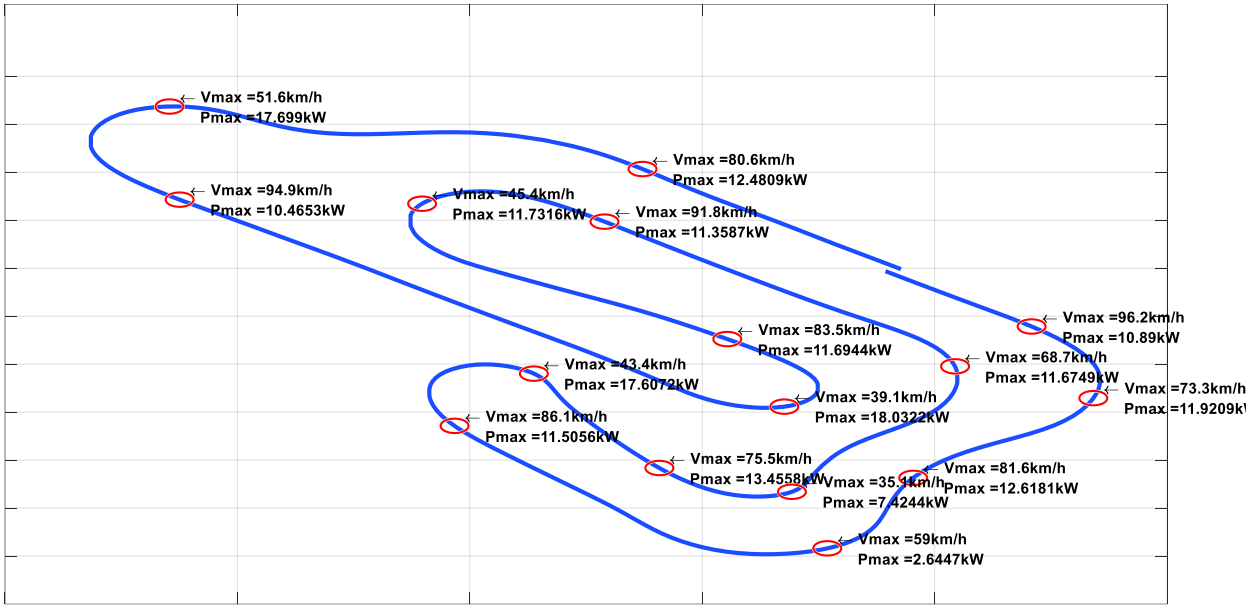

Figure 3. 8 E-Kart track layout

Similar assumptions to FE simulation are used to simulate the E-kart race using the power and energy profile in Figure 3. 9, and it is assumed that the car is always in motion, ignoring the race start and pit-stop. There are seven discharge pulses of varying duration, with the longest one almost lasting 8.5 seconds, between the region of no power application during the braking into the corner. The power is zero because of the aforementioned assumption that regeneration is assumed to be zero. The power profile will vary from track to track and the race condition, but the data analyzed is a good estimator of the E-kart's track behavior, allowing to estimate the power and energy requirements to perform analysis to design the battery pack.

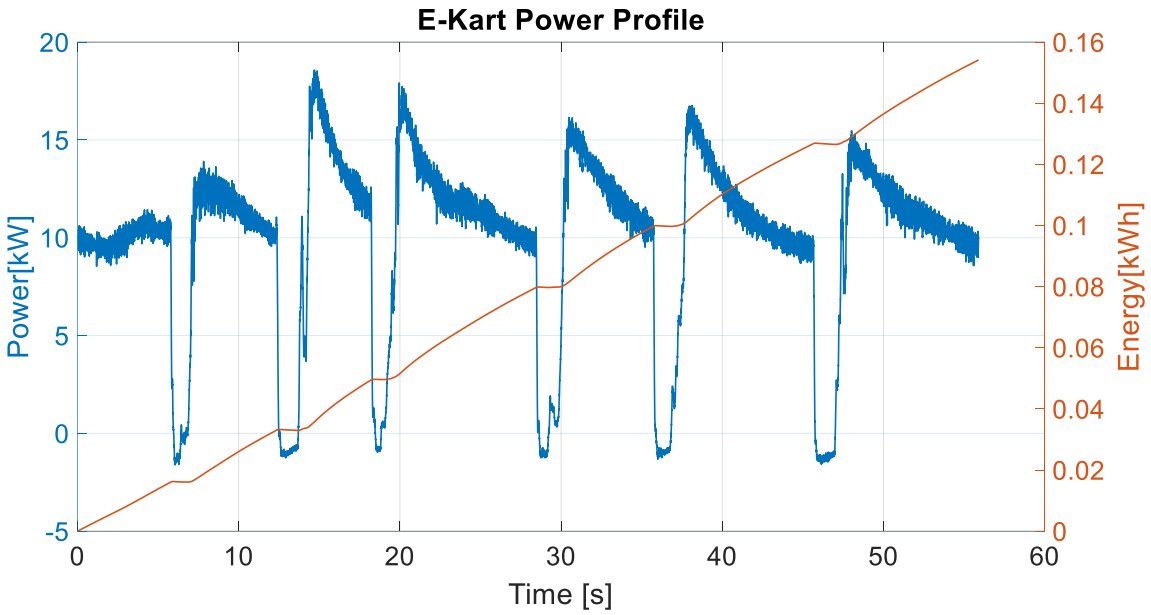

Figure 3. 9 30hp E-Kart power and energy profile for 1 lap

3.3 Hill Climb and Time Trial Racing (HCTTR)

HCTTR is one of the oldest forms of racing in which the driver races against the clock. Hill climbs are about beating the clock while climbing up a hill in a racing vehicle. The data analyzed for this category of motorsports is provided by the Buckeye Current racing team at the Ohio State University. The team has been competing in the HCTTR since its inception in 2010. The team scored two consecutive podiums at the Isle of Man TT Zero (IOMTT) in 2013 and 2014 and three consecutive podiums at Pikes Peak International Hill Climb (PPIHC) in 2015, 2016, and stepped on top spot in 2017. HCTTR are very different from close circuit racing introduced in the open-wheel racing section. The major difference in the duty cycle is the periodic nature of closed-circuit racing, as the duty cycle is redundant for every lap, compared to the aperiodic nature of the duty cycle for HCTTR, as the driver drives from point A to point B without repeating any section of the track.

3.3.1 PPIHC

PPIHC, also known as the race to clouds, is a 19.99km long hill climb with 156 corners and an elevation gain of 1422m located in America's Mountain in Colorado, USA [24]. The start line is at the mile 7 marker of the Pikes Peak Highway and ends at the summit of the mountain. The self-sanctioned race event sees a diverse turnout and attracts everyone from a small team of students to multinational automotive manufacturers such as Volkswagen. The biggest challenge of PPIHC is the elevation change; with a decrease in air density, the internal combustion engines can lose up to 30% of its power as well as the thin air takes a toll on the drivers [24]. Electric vehicles are better suited for this race as the performance is not dependent on the air density rather the driver. The overall hill climb record of 7:57.148 is held by a purpose-built Volkswagen ID. R, the motorcycle record of 9:44.963 by the Aprilia Tuono V4 1100.

Buckeye Current RW-3 X2:

The RW-3 X2 is a 258hp electric motorcycle that helped the Buckeye Current team to reach the top step of the podium in 2017, boasting many upgrades and experience that the team earned in the previous years. The specifications are summarized in Table 3. 4.

Figure 3. 10 Buckeye Current RW-3 X2 at PPIHC in 2017

The motorcycle took 1.3 minutes more than the overall fastest motorcycle, developed by a well-established manufacturer to complete the race. The battery pack is designed with high specific power in interest and enough energy to complete the 11-minute duty cycle.

Racing Series	PPIHC
Weight (kg)	228
Max Speed (km/h)	181.30
Race Duration (min)	11.05
Battery Pack Energy (kWh)	7.7
Battery Pack Power (kW)	217 (Continuous) / 405 (Peak)
Battery Pack Voltage (V)	480
Battery weight (kg)	70.3
Specific Power (W/kg)	3087 (continuous) / 5761 (Peak)
Specific Energy (Wh/kg)	109.53
Cooling system	Air

Table 3. 4 Specifications of RW-3 X2

The power profile in Figure 3. 11 looks much messier than the power profiles in Figure 3. 5 and Figure 3. 9; it is because the former is the profile for the whole race, whereas the latter are the profile for one lap of the race. The data is from the on-board data logger and represents the real race conditions. There is no energy regeneration, and the data is processed to remove the noise without losing any substantial information. As compared to the FE profile, the vehicle does not remain at max power for a long duration due to the nature of the track. The 156 corners of the PPIHC track require constant braking and acceleration effort from the rider, which creates such a variable profile. The peaks tapper off by the end of the profile, indicating a substantial drop in battery pack voltage of power limitation due to high temperature. The team provided no data about the battery pack temperature or voltage; hence it is difficult to comment about the tapering-off of power at the end. The motorcycle consumed 84% of pack energy to complete the duty cycle.

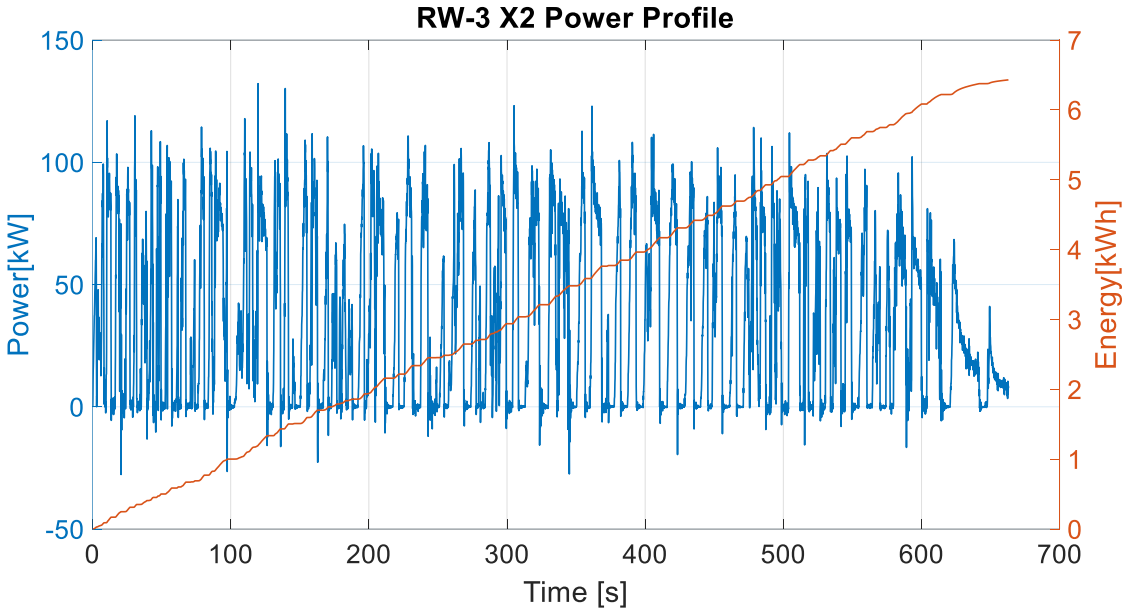

Figure 3. 11 RW-3 X2 power and energy profile

3.3.2 IOMTT

Figure 3. 12 RW-2 X1 raced by Buckeye Current at IOMTT in 2014

IOMTT is one of the most beautiful and dangerous motorsports events in the Isle of Man, a tiny country between England and Ireland, over two weeks of practice and race sessions. The course is 60.72km long, with an elevation gain of 396m [25]. The road course consists of over 200 corners, and the lap record for the electric motorcycle is 18:34.172, set by team Mugen in 2018. The

Buckeye Current team raced in IOMTT in 2013 and 2014, achieving third place with the lap time of 25.02 minutes and 24.12 minutes, respectively. The data used for the analysis is from an IOMTT concept simulation with a much bigger battery pack that the team was developing before the event was canceled. The simulation assumes an ideal 600 V 27 kWh battery. The vehicle specifications are summarized in Table 3. 5.

Racing Series	**IOMTT**
Weight (kg)	250
Max Speed (km/h)	320
Race Duration (min)	17.37
Battery Pack Energy (kWh)	27
Battery Pack Power (kW)	127 / 153
Battery Pack Voltage (V)	600
Battery weight (kg)	131
Specific Power (W/kg)	969.5 / 1168
Specific Energy (Wh/kg)	206
Cooling system	Thermal Mass

Table 3. 5 Specifications of the IOMTT concept

The profile is quite similar to the RW-3 X2 profile, except for it being generated by a simulator. There is no regeneration, and the power does not taper off by the end of the profile as ideal conditions for the battery and powertrain are assumed. There are more pulses as compared to PPIHC because of more corners.

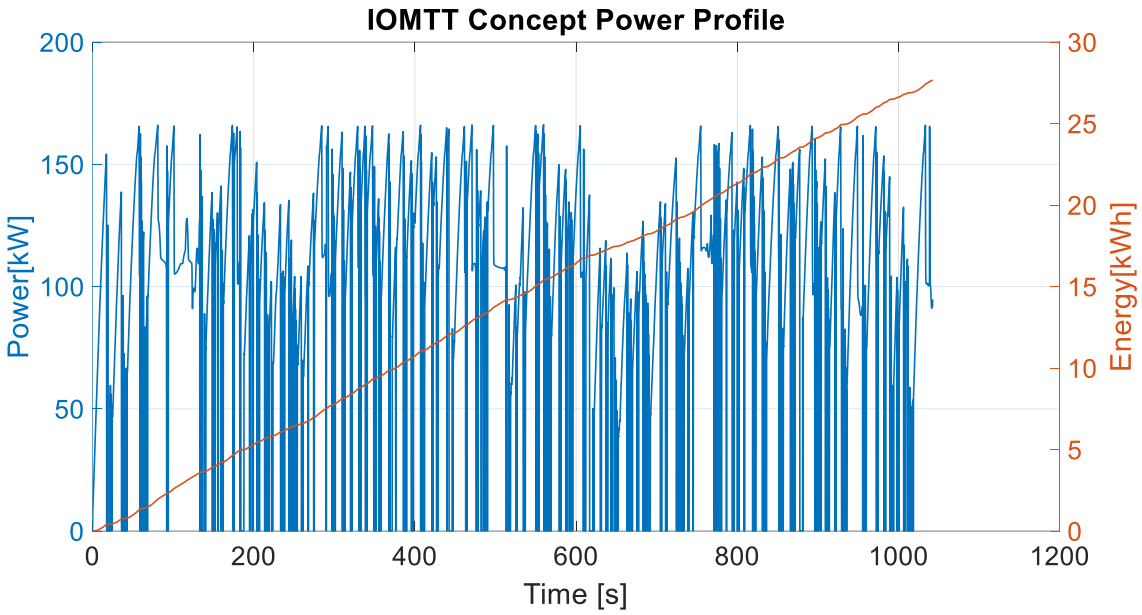

Figure 3. 13 IOMTT concept power and energy profile

3.4 Land Speed Racing

A land speed racing vehicle's objective is to achieve the highest possible speed in a straight line without losing contact between the ground and the tires. The rules and regulations are lax compared to open-wheel racing; to be considered a car, the vehicle should have four wheels, and to be considered a motorcycle, the vehicle should have two wheels with the rear wheel propelled by a prime mover. The vehicles are further subdivided into classes depending on the weight, size, and bodywork. To be considered as a world land speed record, the vehicle should perform two runs in the opposite direction within two hours of the first-run, according to FIA and FIM. The average of the timed miles of two runs is used to determine the final speed.

The Bonneville salt flats in Utah, USA is the Mecca of land speed racing; motorsports enthusiasts and professional racing teams have flocked to this expanse since the 1930s because of its flat and smooth surface that extends as far as the eye can see. Venturi Buckeye Bullet 3 (VBB3)

set the world's fastest land speed record in 2016 with the 549.43km/h at the Bonneville salt flats, and the Venturi Voxan Wattman aims to break the FIM land speed record of 330km/h in the near future.

3.4.1 VBB3

Figure 3. 14 Venturi Buckeye Bullet at Bonneville Salt Flats, Utah

The Buckeye Bullet is one of the longest-running motorsports projects at Ohio State University; it started with the Formula Lightning team looking for a new adventure after the conclusion of the electric open-wheeled collegiate racing competition in the year 2000. The Buckeye Bullet (BB) 1 achieved 506.88km/h in 2004 using NiMH batteries, and the BB2 averaged 487.43km/h in 2009 using a powertrain powered by the hydrogen fuel cell. The VBB2.5 attained a speed of 495.14km/h in 2010. The current iteration, VBB3, is still the world's fastest electric vehicle. The vehicle specifications are summarized in Table 3. 6.

Racing Series	FIA Land Speed Racing [VBB3]
Weight (kg)	3600
Max Speed (km/h)	549.43
Race Duration (min)	>2
Battery Pack Energy (kWh)	92.4
Battery Pack Power (kW)	2200
Battery Pack Voltage (V)	800
Battery weight (kg)	317.15
Specific Power (W/kg)	
Specific Energy (Wh/kg)	

Table 3. 6 VBB3 Specifications

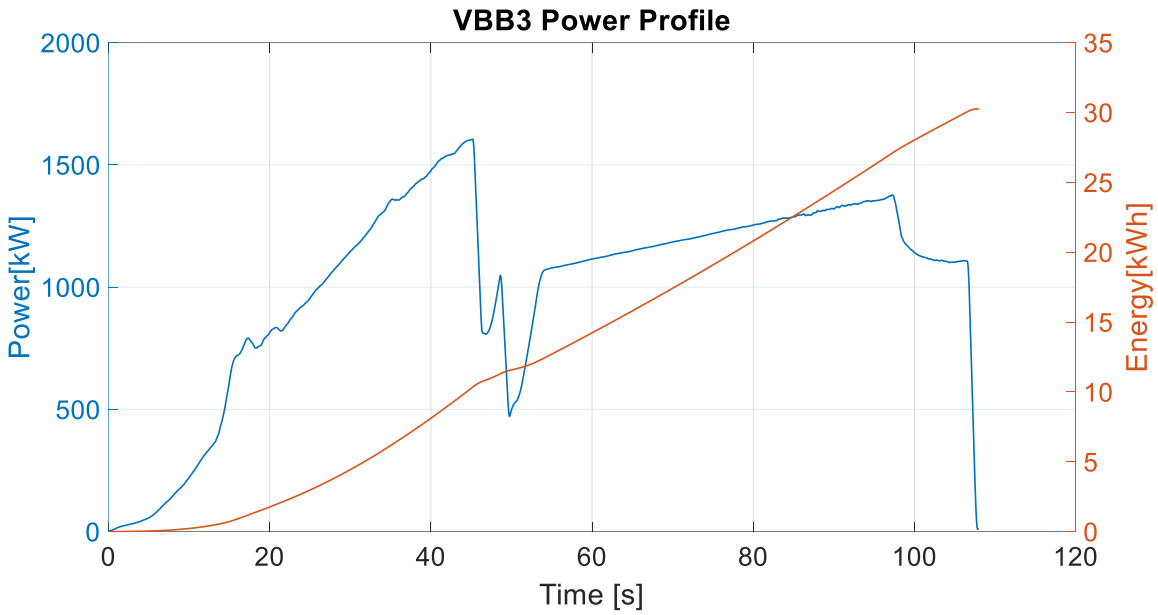

Figure 3. 15 VBB3 power and energy profile

The power and energy profile for VBB3 in Figure 3. 15 is from the vehicle's data logger; the data was acquired in 2016 during one of the record-setting runs. The profile is much simpler as compared to the previous profiles as the driver is expected to drive in a straight line as fast as possible. The change in the power profile slope between 0 and 40 seconds happens as the driver tries to find the grip and limit wheel slip. The drop in power between 40 and 60 seconds results from gear change, the vehicle is equipped with a two-speed gearbox, and the race strategy dictates

the power drop. The power increases linearly after the drop until the mile marker for brake application is reached. The energy consumption is linear, and a total of 30.25kWh of energy is consumed in one run. The vehicle needs at least 61kWh of energy to satisfy the energy requirements for two runs.

3.4.2 VVW

Figure 3. 16 Three iterations of VVW

VVW is a high-performance motorcycle developed by Voxan Motors, a subsidiary of Venturi Automobiles. The chassis and the drivetrain are developed by Venturi, and the battery pack by the Center for Automotive Research at OSU. The motorcycle boasts a 270kW motor and a 15kWh battery pack. The three motorcycles in Figure 3. 16 are three iterations of the motorcycle, with the only difference being the bodywork. FIM segregates the motorcycles according to the weight and type of bodywork; the one on the left is considered fully naked, whereas the one on the right is partially faired as the driver's side profile is completely visible during the race. The motorcycle broke the FIM World Land Speed record in November 2020. The vehicle specifications are summarized in Table 3. 7.

Racing Series	FIM Land Speed Racing [VVW]
Weight (kg)	300
Max Speed (km/h)	320
Race Duration (min)	~2
Battery Pack Energy (kWh)	15
Battery Pack Power (kW)	~250
Battery Pack Voltage (V)	800
Battery weight (kg)	150
Specific Power (W/kg)	1667
Specific Energy (Wh/kg)	100
Cooling system	Forced Air

Table 3. 7 Specifications of VVW

The power and energy profile in Figure 3. 17 is from the simulator developed to estimate the power requirements to break the land speed record. The power and energy profiles are similar to the profile for VBB3 without the gear shift. Each run requires 5kWh of energy and a total of 10kWh to complete the race.

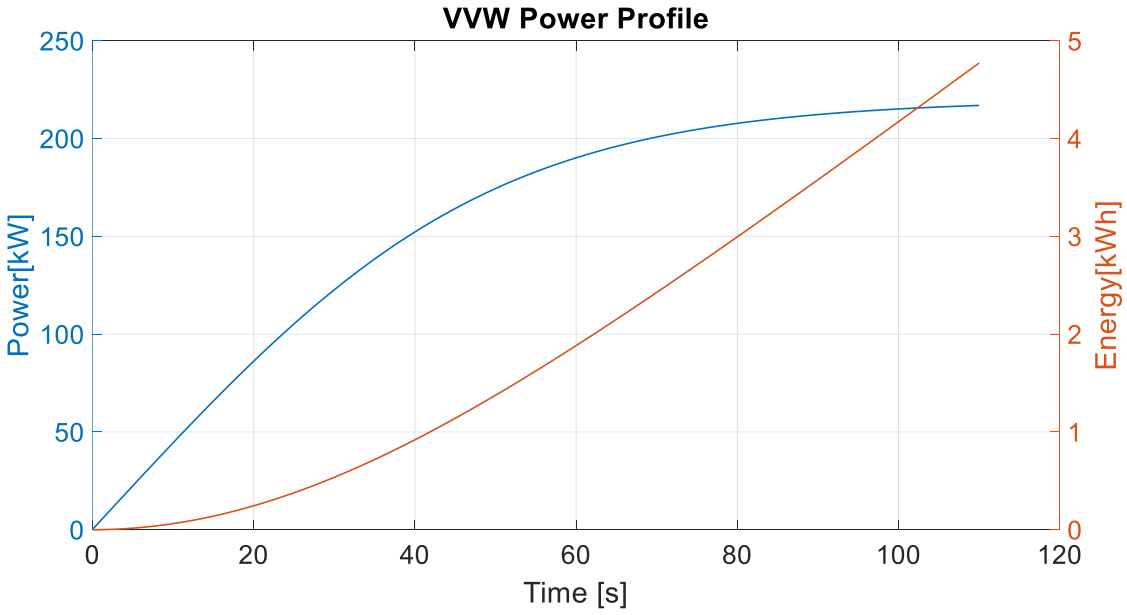

Figure 3. 17 VV3 Power and energy profile

Chapter 4: Generalized Methodology and Metrics

To develop a generalized approach to the design of energy storage systems for a diverse range of motorsports, it is crucial to develop a generalized algorithm to study data; this section describes the generalized approach and metrics used to study and analyze data from various sources.

4.1 Methodology

The generalized mythology is summarized in Figure 4. 1; the first step is to acquire data from multiple race teams competing in different race categories. After acquiring data, it is qualitatively analyzed and categorized to develop a generalized methodology, which uses statistical metrics derived from the battery power profile analysis. The results from the next section's metrics help in choosing cell chemistry and designing the energy storage system.

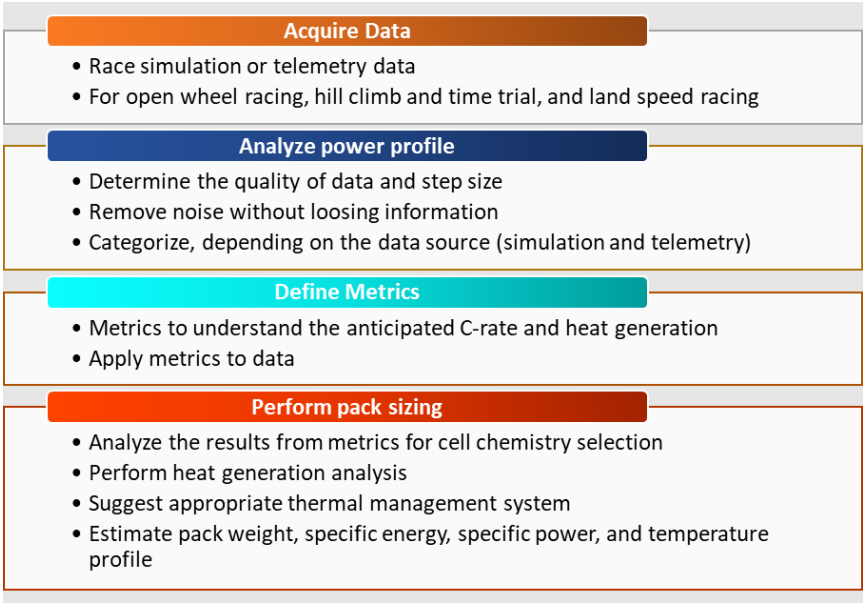

Figure 4. 1 Generalized Methodology

Acquiring data is one of the most challenging steps of the methodology as motorsports teams are highly protective of the race data. It is easier to procure data from independent software providers or colligate teams participating in the motorsport category. The data sources used for the thesis are summarized in Table 4. 1.

Race	Data Source	Data Logging	Step Size
Formula E	Canopy Simulations	Simulation	Variable step
E-kart	The University of Cassino and Southern Lazio, G-Side racing	Race test	0.0010
PPIHC	Buckeye Current	Race	0.1
IOMTT		Simulation	0.2
VBB3	Center for Automotive Research at the Ohio State University	Race	1
VVW		Simulation	0.01

Table 4. 1 Data source

Three of the profiles analyzed are from the data logger of the race vehicle and three from race simulations, which do not account for dynamics of Li-ion cells, i.e., the change in the open-circuit voltage of the battery pack with respect to change in the SOC and temperature of the battery pack. Albeit the data is a good estimator of the required battery performance.

The varied data sources and data accusation methods across the board propose a data analysis problem as the step sizes and data quality is different; the second step in the methodology is to qualitative analyze the data by plotting the power profiles and making sure that the plotted data matches with the vehicle specifications. For example, the data for the PPIHC showed some regeneration, but the team acknowledged that there is no regeneration, and it is noise. Two different algorithms are developed to analyze the simulation and race data, as the race data require some pre-processing to eliminate the noise without losing any information. The next step after processing and categorizing the data is to define metrics to study data.

4.2 Defining Metrics:

Various metrics are defined to study the battery pack power profiles, which help in selecting the most appropriate cell chemistry and design the battery pack are explained using one lap FE power profile:

Max, Mean, and Standard deviation of Power:

The max, mean, and standard deviation of various power profiles are calculated to understand the battery pack's power requirements and evaluate a few metrics defined further in this section.

Normalized power:

The power profile is normalized by:

$$Normalized\ power = \frac{Power(t)}{Max\ power} * 100$$

Dividing power at a given time by the absolute maximum power observed in the power profile. The FE power profile is normalized in Figure 4. 2.

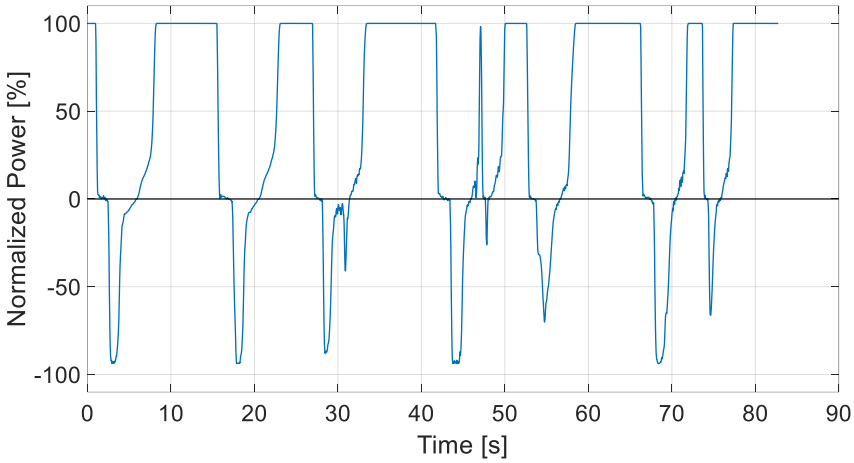

Figure 4. 2 Normalized FE power profile

Normalized energy consumption:

Energy consumed in the normalized power % range divided total energy consumed during the duty cycle, or energy consumed in a C-rate range divided by the total energy consumed.

$$\frac{Energy\ consumed}{Total\ Energy} * 100$$

The metric gives an estimation of energy consumed in a given normalized power or CR_P range and visualize energy consumption.

C-rate of Power Profile:

C-rate is a measure of the rate of charge or discharge of the battery pack. It is calculated by Power at a given time divided by the total energy consumed to complete the duty cycle. Note that this is a modified version of the traditional C-rate calculated based on current and battery capacity.

$$CR_P(t) = \frac{Power(t)}{Energy\ consumed}$$

C-rate is denoted by $CR_P(t)$, it is an estimator of the charge and discharge current that the battery pack is expected to sustain for a given power profile. It is further divided into continuous and peak charge/discharge C-rate, defined in the following sections. The one-lap duty cycle is represented as $CR_P(t)$ for FE in Figure 4. 3. $CR_P(t)$ greater than zero denote discharge current, and less than zero denote charge current.

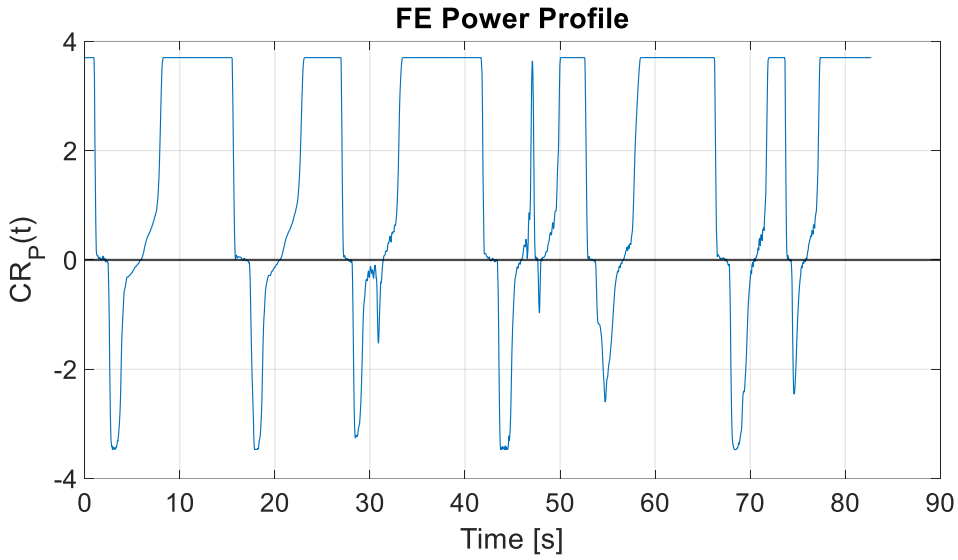

Figure 4. 3 FE C-rate profile

Continuous C-rate of Power Profile:

The continuous C-rate of a battery pack is the maximum current at which the battery pack can be charged/discharged continuously until the pack reaches maximum charge potential/runs out of energy. Usually, the continuous charge/discharge duration is limited by the cell manufacturer to prevent overcharging and excessive discharge. Continuous C-rate is calculated by averaging $CR_P(t)$ for the duty cycle of the vehicle and denoted by $Continous\ CR_P$.

$$Continous\ CR_{P,ch} = \frac{\sum_{CR_P(t)<0} CR_P(t)}{N_{sample}}$$

$Continous\ CR_{P,dis} = \frac{\sum_{CR_P(t)>0} CR_P(t)}{N_{sample}}$ The mean of $CR_P(t)$ is calculated for charge and discharge, in case of FE mean of $CR_P(t)$ less than zero is continuous charge C-rate and mean of $CR_P(t)$ greater than zero is continuous discharge C-rate as represented in Figure 4. 4.

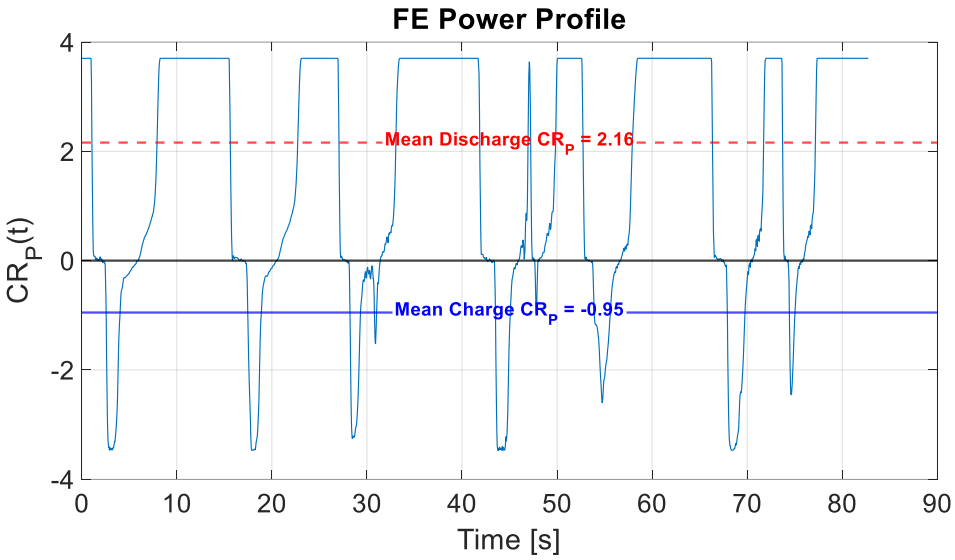

Figure 4. 4 FE continuous CRP(t)

Peak C-rate of Power Profile:

Peak C-rate is the maximum charge/discharge current that the battery cell can sustain for a short period defined by the manufacturer, usually about 10 seconds and 30 seconds. Peak C-rate can be substantially higher than the continuous C-rate. Charging/discharging battery cells at peak C-rate over the specified duration can damage the cell permanently. $Peak\ CR_P(t)$ is defined as $CR_P(t)$ pulse with a magnitude greater than the $Continous\ CR_P(t)$ and a duration of over 0.2 seconds.

The pulses for the FE power profile are highlighted in Figure 4. 5. The cell chemistry chosen for this power profile should be able to sustain a continuous charge and discharge $CR_P(t)$ pf -0.95 and 2.16 with the ability to sustain the repetitive highlighted pulses in Figure 4. 5 with varying durations.

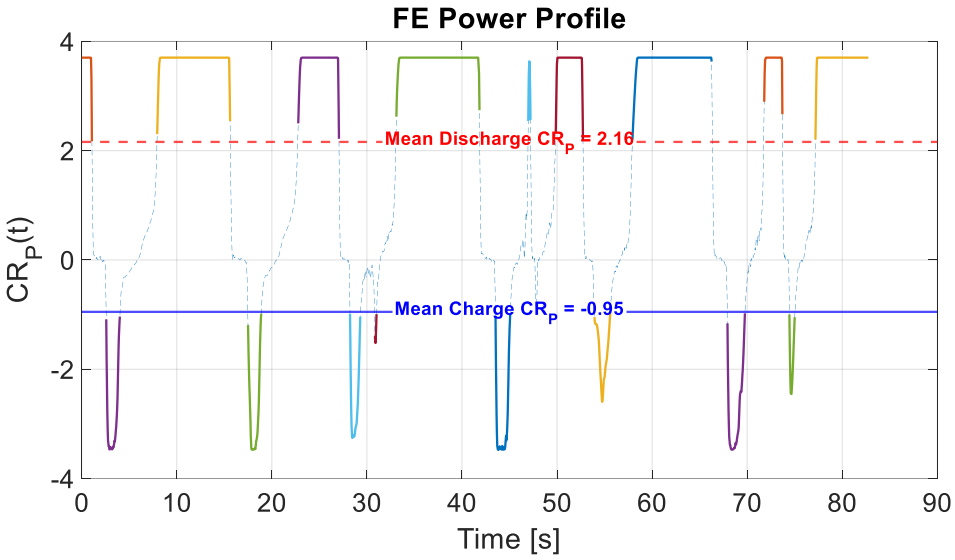

Figure 4. 5 Peak CRP(t)

The $Continous\ CR_P(t)$ and $Peak\ CR_P(t)$ are the two most crucial metrics that help choose the most optimal cell chemistry for a power profile.

Max peak $\boldsymbol{CR_P}$:

Max peak CR_P is the absolute maximum CR_P observed for a set of pulses for a given power profile. For FE discharge profile, the maximum CR_P for all the pulses is 3.7 from Figure 4. 6. For the charge profile, the Max peak CR_P is -3.5.

Min peak $\boldsymbol{CR_P}$:

Min peak CR_P is the absolute minimum CR_P observed for a set of pulses for a given power profile. For FE discharge profile, the min CR_P for all the pulses is 3.6 in green from Figure 4. 6. For the charge profile, the min peak CR_P is -1.5 in purple.

Mean peak $\boldsymbol{CR_P}$:

Mean peak CR_P is the absolute mean of the maximum amplitude of each pulse that occurs during a given power profile. For FE profile, mean peak CR_P for discharge is 3.69 and -2.74 for charging.

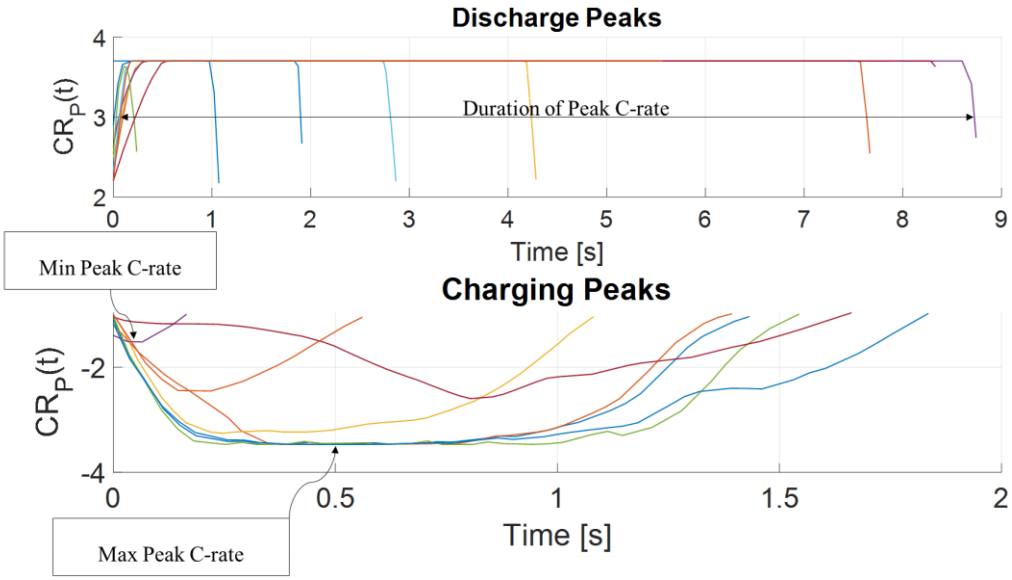

Figure 4. 6 FE power profile peaks

Duration of Peak C-rate:

$Peak\ CR_P\ Duration$ is the duration of each pulse for a given power profile.

$$Peak\ CR_P Duration = \ Peak\ CR_P(t_\infty) - Peak\ CR_P(t_0)$$

Figure 4. 6 represents the nine discharge peaks and eight charge peaks observed in Figure 4. 5. The width of each peak is the duration of the pulse for charge and discharge. The selected cell chemistry should sustain the continuous and peak C-rates to be suitable for a given application. For one lap of FE, the maximum $peak\ CR_P\ duration$ for discharge is 8.7 seconds at max $peak\ CR_P$ equal to 3.7, for charging the maximum $peak\ CR_P\ duration$ is 1.83 seconds with $max\ peak\ CR_P$ equal to -3.5. The chosen chemistry must suffice both the charge and discharge $Peak\ CR_P(t)$.

Total Duration of Peak C-rate

$Total\ Peak\ CR_P\ Duration$ is equal to:

$$Total\ Peak\ CR_P Duration = \sum Peak\ CR_P\ Duration$$

The sum of the duration of all the pulses observed in Figure 4. 6. The higher the $Total\ Peak\ CR_P\ Duration$, the higher would be heat generated because of ohmic losses. This metric will help choose the right cell chemistry with the lowest resistance and thermal management system for a given profile. For example, if the total duration is very short, then the battery pack's thermal mass could be used as a passive thermal management system, albeit if it is long, then the battery pack might require an active thermal management system.

Occurrence of Peak C-rate

$CR_P\ Occurance$ is the number of $CR_P(t)\ peaks$ for charge and discharge over the duration of the power profile. In Figure 4. 5, $N_{peaks} = 9$ for the discharge and $N_{peaks} = 8$ for charging. The

Ohmic losses calculated by I^2R where I is current and R is internal resistance, are significantly higher during the peaks, as the current is higher, hence the increase in the occurrence of peaks in a power profile will lead to an increase in the heat generated over the duration of the duty cycle. If multiple cell chemistries suffice the continuous and peak $CR_P(t)$ requirements, the chemistry with a lower internal resistance will be better suited for a power profile with a large number of peaks. On the other hand, if the profile is much more uniform, then chemistry with a higher resistance but a lower price could be used.

Square of $\boldsymbol{CR_P}$:

The heat generated during charge/discharge of a battery pack is calculated by I^2R. C-rate is the rate of charge/discharge; hence the square of C-rate is an estimator of heat generated. ${CR_P}^2$ is directly proportional to heat generated and helps in comparing the energy wasted as heat independent of resistance for various power profiles.

$$ {CR_P}^2 = \frac{\sum Max\ peak\ CR_P}{Occurance\ of\ Peak\ CR_P} $$

Chapter 5: Results and Analysis of Formula E race power profile

The metrics defined in the previous chapter are used to analyze all the vehicles described in chapter three to evaluate the most feasible cell chemistry for the application. In this chapter, the whole process of metric application and evaluation of the power profile is explained using the FE power profile, and the results for all the power profiles are summarized at the end of the chapter.

The eleven race profiles in mentioned Figure 3. 4 are randomly concatenated to form a 33-lap race simulation, equivalent to a race duration of 45 minutes and an additional lap. The resultant simulated power profile is shown in Figure 5. 1. The total race duration is 2,795.8 seconds or 46.59 minutes, and the energy consumed to complete the race is 53.99kWh. The simulation results are summarized in table Table 5. 1,

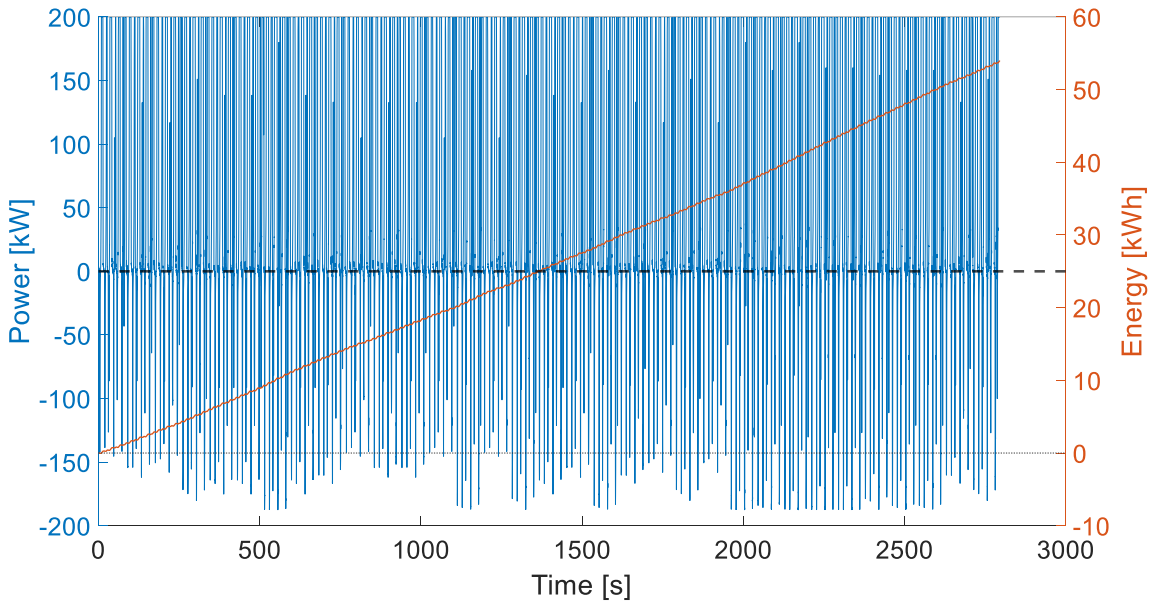

Figure 5. 1 FE race power and energy profile

Metric	Formula E
Duration (min)	46.597
Distance (km)	97.040
Peak Power (kW)	199.953
Mean power (kW)	116.627
SD power (kW)	113.172
Peak Regen Power (kW)	-187.455
Mean Regen Power (kW)	-90.351
SD Regen Power (kW)	59.452
Total Energy. (kWh)	53.994

Table 5. 1 Summary of race simulation

The power profile is normalized and broken down in normalized power range to visualize the power application duration and energy consumption in Figure 5. 2 and Figure 5. 3. The normalized power for FE extends from -100% to 100%, and regeneration is denoted by the negative values and discharge by positive values. The range of each segment in the bar graph is 10%, denoted by the mean of the normalized power range. The average discharge power is 58.33% or 117kW, and the average regeneration power is 25.77% or 51.54kW.

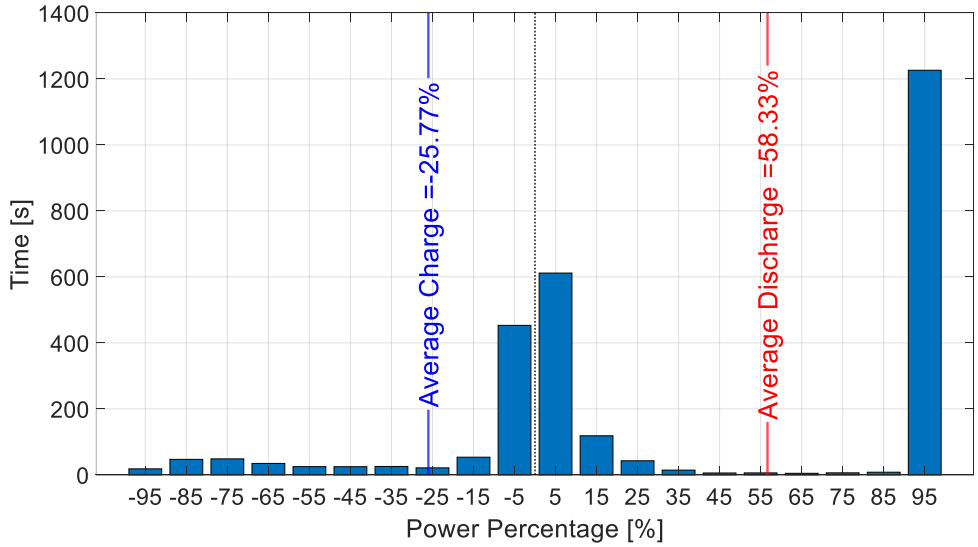

Figure 5. 2 Duration of power application

The FE car drives in the 90-100% power range for 20.43 minutes, or almost half of the race duration, and 0.76 minutes between 30% and 90%. One of the reasons for such disparity in power application duration is that the driver needs to accelerate coming out of the corner and achieve maximum speed possible before slowing down for the next corner, so the drive keeps the foot down to apply 200kW power for as much duration as possible. During braking into the corner, the car recuperates the energy, but it slows down the car. Hence, energy is not recuperated similarly for every lap, and the power goes to the 0-10% power range.

Energy is recuperated for almost a third of race duration or 12.5 minutes during the braking maneuvers. The regeneration power is inversely proportional to the speed of the car; the higher the regeneration, the lower would be the speed of the car at the end of the regen period. The driver tries to remain in the 0% to -20% power range for most of the regen period to avoid slowing down the car too much and maintain high corner exit speeds, albeit higher energy is recuperated even with a shorter duration between -100% and -60% power range.

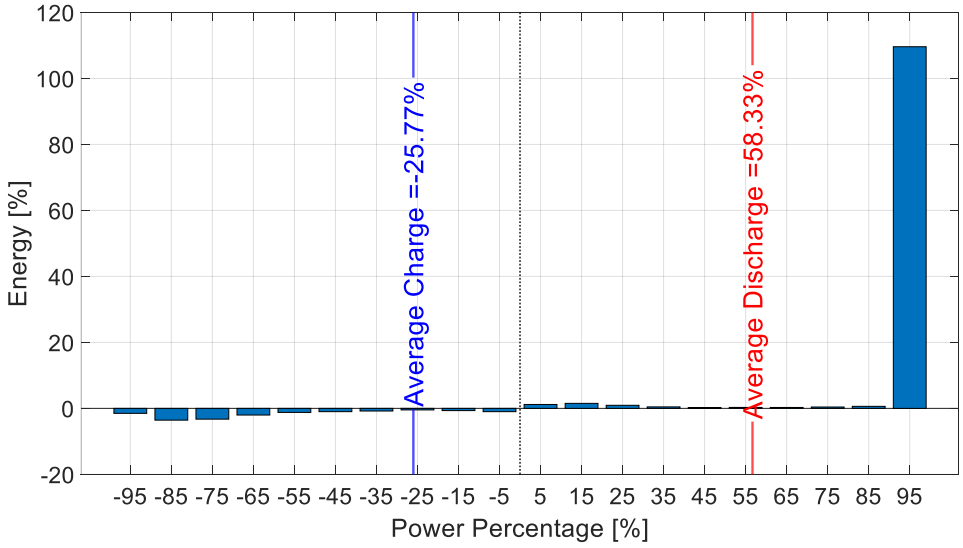

Figure 5. 3 Energy consumption

As the car is driven in the 90-100% power range for half of the race duration, an exponentially higher amount of energy is consumed in the same power region. The vehicles consume 109.6% or 59.184 kWh of energy. During the discharge, the total energy consumption is 115.52% or 60.22kWh, which shows the importance of energy recuperation. The battery pack is limited to 54kWh; the car makes up for the 6.22kWh deficit to complete the race. The energy generated depends more on the power range rather than the duration of regeneration. 5.59kWh out of 6.22kWh is recuperated between -100% and -60% power race even though the vehicle sustains this power range for 2.47 minutes out of 12.5 minutes of regeneration period.

5.1 FE Discharge Power Profile Analysis

The FE C-rate profile is deduced from the simulation results in Figure 5. 1, and the identified metrics are tabulated in Table 5. 2.

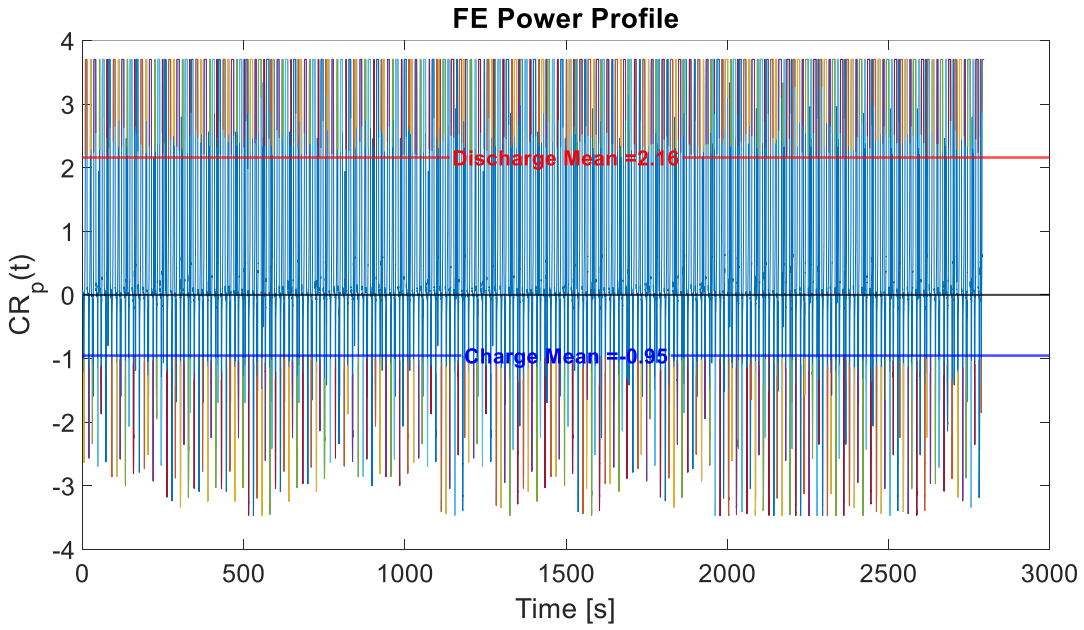

Figure 5. 4 FE C-rate profile

The average discharge C-rate is equal to 2.16C, and the average discharge C-rate is equal to -0.95C. Each of the highlighted peaks for discharge in Figure 5. 4 is plotted in Figure 5. 5 to visualize and understand the max peak C-rate, min peak C-rate, and C-rate duration.

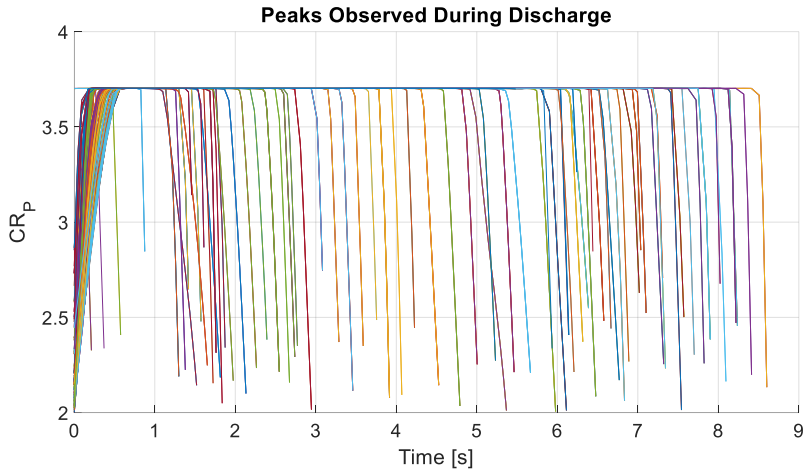

Figure 5. 5 Peaks observed during discharge

The maximum peak C-rate observed is 3.7C with the shortest duration of 1.25 seconds and the longest duration of 8.56 seconds. A total of 239 peaks lasting a total duration of 1117.9 seconds, almost half of the race duration occurs during the discharge. The variation in the maximum amplitude of peak C-rate is minuscule as the mean peak C-rate is equal to 3.64. Very few peaks in the simulation have a maximum peak C-rate lower than 3.7C.

Parameters	Discharge
Total Peak Duration (s)	1117.9
Number of Peaks	239
Mean C-rate total	2.16
Mean peak C-rate	3.64
Max C-rate | Duration at Max C-rate (s)	3.70 | 1.25
Max Duration (s)| C-rate	8.56 | 3.70
Continuous $\boldsymbol{CR_P}$	2.16
Peak $\boldsymbol{CR_P}$	4

Table 5. 2 Summary of evaluated metrics

The C-rate peaks in Figure 5. 5 are further visualized using a bar graph to understand the anticipated behavior of the battery pack and estimate heat generation.

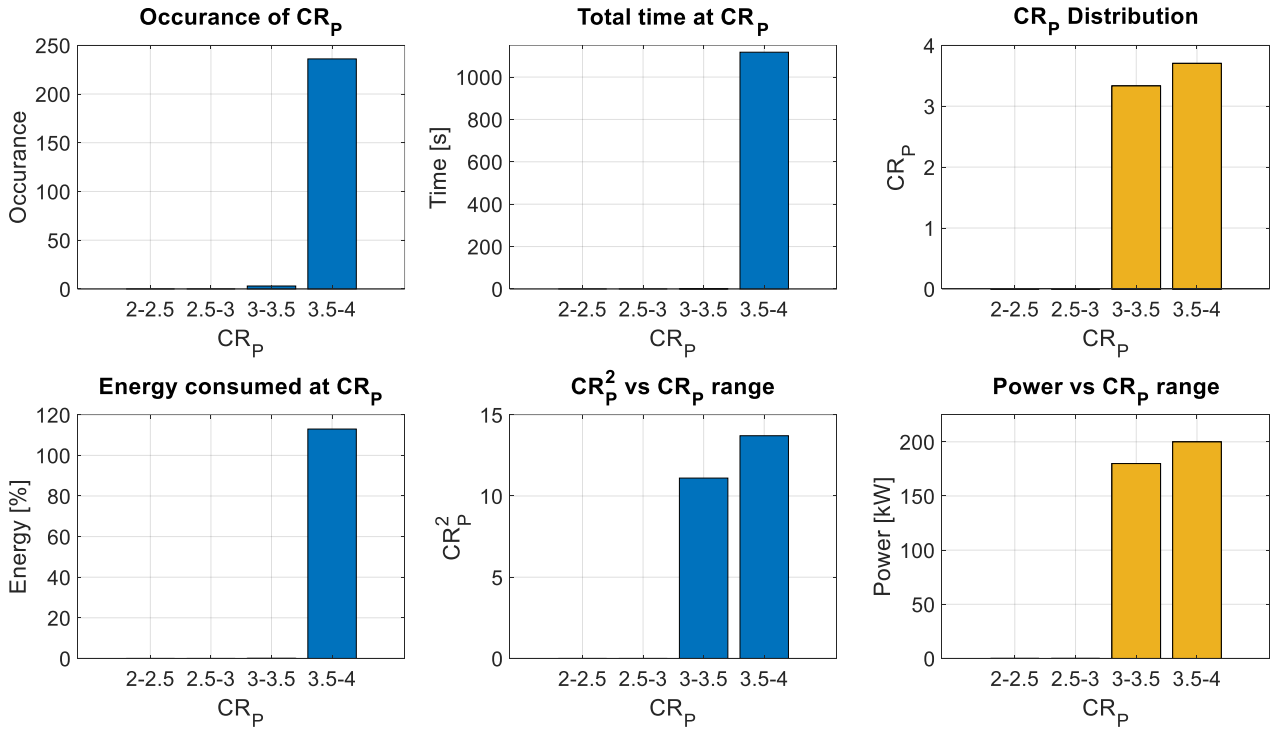

Figure 5. 6 Bar graphs visualizing discharge peak C-rate

No peaks occur between the 2C-3C range, and out of 239 peak C-rate observed in the FE duty cycle, 236 occur in the 3.5C-4C range, and 3 in the 3C-3.5C range, which is synonymous to the discharge pattern in Figure 5. 2. The vehicle remains in the 90-100% power range for most of the duration so that the battery pack will be discharged at the maximum possible C-rates. The battery pack is discharged at C-rate between the3.5C-4C for 1117.3 seconds out of 1117.9 seconds of total peak duration, indicating that the peaks between 3C-3.5C last for an average of 0.2 seconds. Most of the heat generated during the discharge will be at a current draw between 3.5C-4C.

The min, mean, and max C-rate between 3C-3.5C and 3.5C-4C vary at the third decimal place. All peaks between 3.5C and 4C have amplitude around 3.7C, and the 3C-3.5C have amplitude around 3.3C. As the battery pack is discharged at 3.7C for 1117.3 seconds, most of the energy is consumed in the 3.5-4 C-rate range, which is synonymous with the behavior observed in Figure 5. 3. Over 100% of energy is consumed in this C-rate range, which is compensated by energy regeneration. The C-rate squared is highest for the 3.5C-4C range, indicating the highest heat generation at 3.7C discharge. The highest power application is observed in the same C-rate range, and heat generation will be the highest because of Ohmic losses.

For the FE discharge profile, the maximum current is drawn from the pack at the highest C-rate for the longest duration, indicating a large amount of ohmic losses. Integrating the ohmic losses over the duration of discharge will provide an estimate of energy lost as heat and help in choosing the right BTM system to remove the heat and keep the battery pack in the operational temperature range. Heat generation is also highly dependent on the resistance of cell chemistry. The peak C-rate and the continuous C-rate from the power profile are used to choose the appropriate cell chemistry in the following section.

5.2 FE Charge Power Profile Analysis

The charging profile is different from the discharge profile as it is more irregular, and the maximum peak C-rate values vary more as compared to the discharge profile. The mean charge C-rate is -0.95, which is less than half of the mean discharge C-rate. There are 224 peaks throughout the duration of the power profile with the max peak C-rate equal to -3.47C with a

duration of 1.52 seconds. The continuous CR_P expected from the battery pack is 1C, and the peak CR_P is 3.5C. The metrics evaluated from Figure 5. 4 FE C-rate profile are tabulated in Table 5. 3.

Parameters	Discharge
Total Peak Duration (s)	285.77
Number of Peaks	224
Mean C-rate total	-0.95
Mean peak C-rate	-2.27
Max C-rate | Duration at Max C-rate (s)	-3.47 | 1.52
Max Duration [s] | C-rate	1.92 | -3.18
Continuous $\boldsymbol{CR_P}$	-1
Peak $\boldsymbol{CR_P}$	-3.5

Table 5. 3 Summary of evaluated metrics

The total duration of discharge peaks is a tenth of the race duration and almost a fourth of the total discharge peak duration. The peaks are also much shorter than the discharge peaks, the longest one lasting shy of 2 seconds. The variability in the maximum peak CR_P is visible in Figure 5. 7; almost all the peaks for the discharge profile were saturated in the 3.5C-4C range, whereas the peaks are much more distributed for regeneration. The regeneration modulation by the driver to maintain a healthy balance between the corner exit speed and energy regeneration results in such high variability. The other interesting dissimilarity between the charge and discharge profile is the time for which $CR_P(t)$ is constant at max peak CR_P. To achieve the maximum possible speed and acceleration, the driver applies the maximum power for as long as possible, whereas the braking maneuvers are much shorter, resulting in much shorter durations for which the $CR_P(t)$ is constant at max peak CR_P.

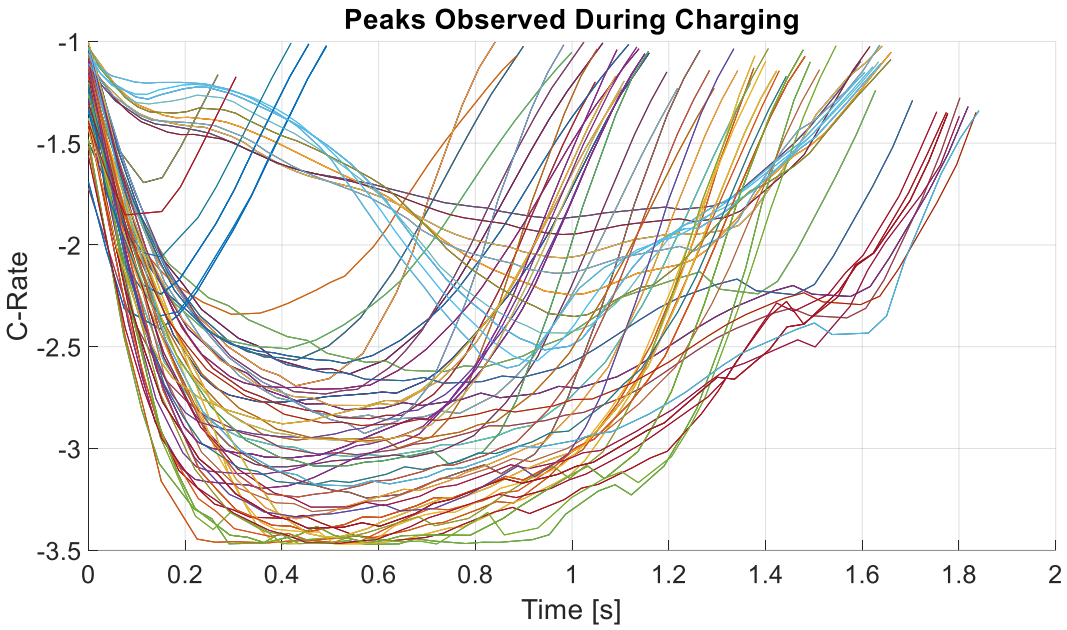

Figure 5. 7 Peaks observed during regeneration

For ease of visualizing the data, the absolute range is presented in Figure 5. 8, albeit it represents charging. Out of 224 charging peaks, 89 occur between 3C-3.5C, 32 between 2.5C-3C and 32 between 2C-2.5C, and 14 between 1.5C-2C and none between 1C-1.5C. The average pulse duration is the longest for 2.5C-3C, lasting 3.21 seconds, followed by 1.44 seconds for the 3C-3.5C range and 1.01 seconds for 2C-2.5C, and 0.94 seconds for 1.5C-2C. The total peak duration is the highest for the 3C-3.5C range because more peaks occur between this range. Most of the energy recuperation in the 3C-3.5C range occurs at the end of straights in Figure 3. 6 as the driver brakes from 200km/h to slower speed to enter the corner, the duration of the braking event is short, albeit the high C-rate helps in recuperating a substantial amount of energy as almost 10% of energy is recovered in the same C-rate range, followed by 6.3% in 2.5C-3C range, and 1.73% and 0.60% in 2C-2.5C and 1.5C-2C, respectively.

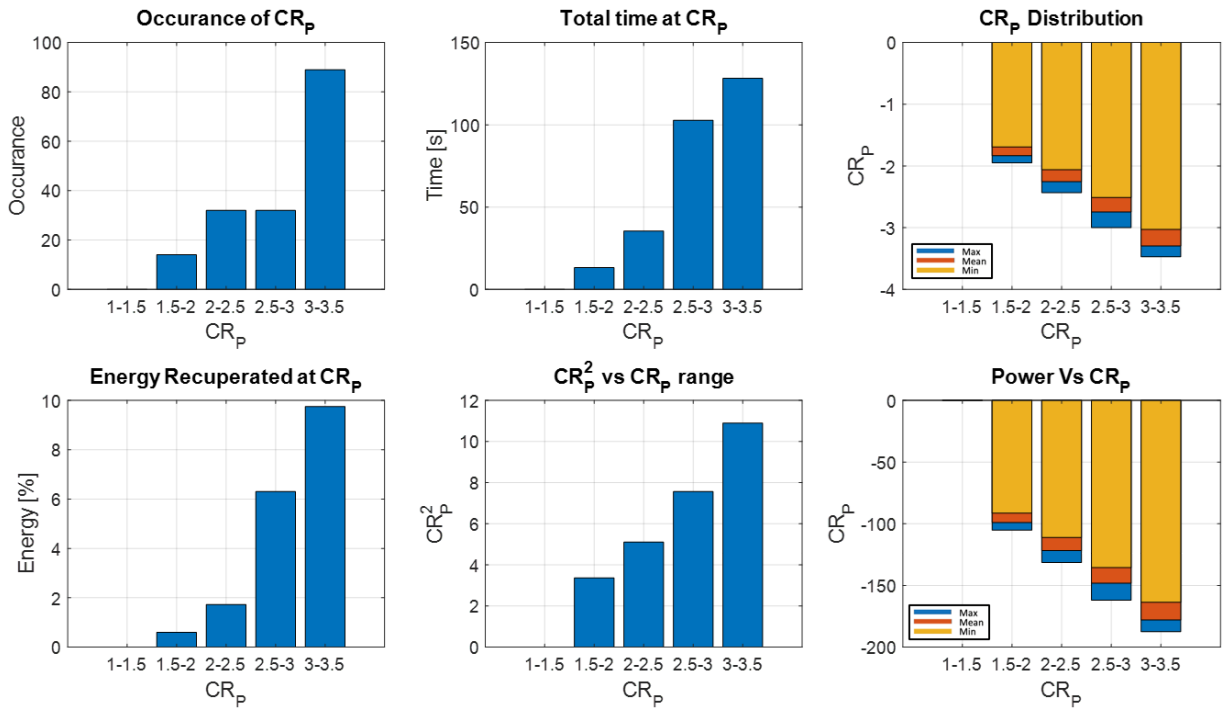

Figure 5. 8 Bar graphs visualizing charge peak C-rate

The C-rate variation is much more evident, as in Figure 5. 7 and CR_P distribution in Figure 5. 8, due to variation in braking power at different corners. The heat generated during regeneration is lower than the heat generated during discharge, as CR_P^2 values are lower when compared to CR_P^2 values for discharge.

5.3 Cell Selection

The three most important metrics for cell selection are the max peak CR_P, the maximum duration of peak CR_P, and mean CR_P or continuous CR_P for both charge and discharge. The three metrics for FE are tabulated in Table 5. 4

Operation	Metric	Value
Discharge	*Max Peak CR_P*	3.70C
	Max Peak CR_P duration	8.56s
	Continuous CR_P	2.16C
Charge	*Max Peak CR_P*	-3.5C
	Max Peak CR_P duration	~2s
	Continuous CR_P	1C
	Duty Cycle Duration	46.59 min
	Energy	54kWh

Table 5. 4 Metrics for Cell selection

The selected cell should be able to suffice the values for metrics in Table 5. 4 at the cell level to suffice the duty cycle for the FE race. The C-rate at the cell level is the same as the C-rate at the pack level; hence it is the best parameter to select the right chemistry. For the FE, the minimum requirement is that the cell chemistry should be cable of discharging at a continuous C-rate of 2.16C with a peak C-rate of 3.7C and peak C-rate duration of almost 9 seconds. The cell should be capable of charging at 1C and sustain a peak charge rate of 3.5C for at least 2C.

Some of the available zero-order cell models at the Center for Automotive Research at Ohio State University in Table 5. 5 are used to select the cell chemistry, perform pack sizing analysis, and evaluate heat generation. Sony VTC-6, Efest 18650, Samsung 30T, and A123 26650 satisfy the continuous and peak charge and discharge criteria. Pack sizing and heat generation are performed on these cells in the further section to select the most optimal chemistry for the FE application.

The input to the model is the power profile, battery voltage, SOC range, and ambient temperature, assumed to be 25°C, and the output is the predicted battery voltage, current, SOC, and heat generated. The equivalent circuit model is shown in Figure 5. 9 [1,2]. The power delivered

by the pack is dependent on m_e and n_e. m_e is the number of cells in series and depends on the battery pack voltage and cell voltage range. n_e is the number of cells in parallel and depends on total energy required for mission profile, peak power request, SOC range, and cell thermal requirements.

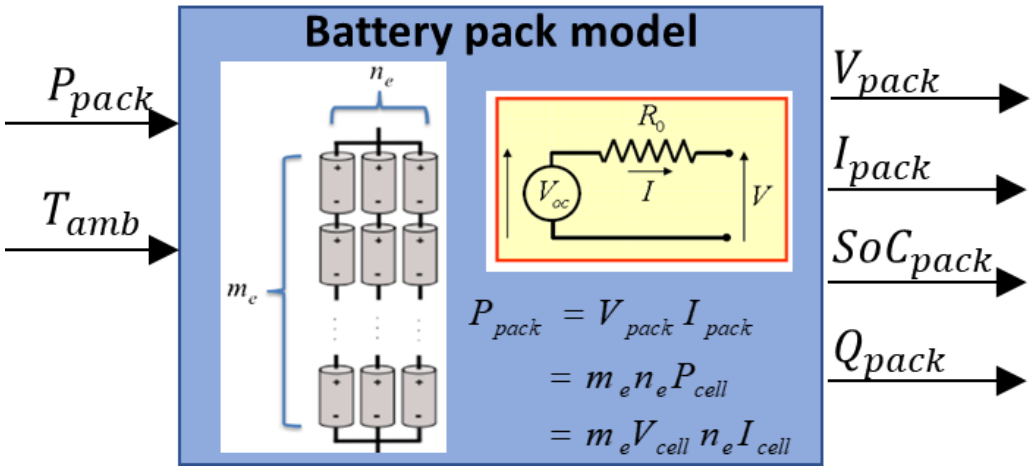

Figure 5. 9 Zero-order equivalent circuit model [1,2]

Manufacturer		Sony VTC-6	Kokam	Efest	Samsung 30T	A123
Format		18650Cyl.	Pouch	18650 Cyl.	21700 Cyl	26650 Cyl
Chemistry		NMC	H-NMC	LMO	NMC	LFP
Weight	g	47	173	47	69	76
Nominal capacity	Ah	3.0	12.0	3.5	3.0	2.5
Nominal voltage	V	3.6	3.7	3.7	3.6	3.3
Voltage range	V	2.5-4.2	2.7-4.2	2.5-4.2	2.5 – 4.2	2 – 3.6
Cont. dch. rate	**C-rate**	**5**	**2**	**2.85**	**11.6**	**20**
Pulse dch. rate	**C-rate**	**10**	**4**	**5.71**		**48**
Cont. ch. rate	**C-rate**	**1**	**1**	**1.14**	**1.33**	**4**
Specific energy	Wh/kg	232	257	278	-	-
Specific power	W/kg	1159	513	794		
Dch. int. res.[2]	$m\Omega$	35	10	51	19.2	24
Dch. pulse power	W	91	278	60	161	

Table 5. 5 Properties of cell chemistries evaluated

5.3.1 Pack sizing and Heat generation analysis for FE

Battery pack sizing is performed on the SONY VTC-6, Efest, Samsung 30T, and A123 26650 cells because they suffice the metrics mentioned in Table 5. 4. The cells in parallel configuration should have a combined capacity of equal to or greater the 54kWh, and the cells in a series configuration should have nominal voltage around 850V. Maximum power output is calculated by multiplying the estimated open-circuit voltage at 100% SOC by the maximum estimated current from the zero-order battery model. The product of the number of cells in series and parallel is equal to the total number of cells required to build the battery pack, and the product of cell weight and the number of cells is equal to the total weight of the cells required to build the battery pack. The packaging and thermal management system are assumed to weigh around 10% to 30% of the weight of the cells. The lightest of all the battery packs evaluated is selected as low weight is the top priority (Figure 3. 1) when it comes to designing battery packs for motorsports.

Pack Specification	**1**	**2**	**3**	**4**
Cell	Sony VTC-6	Efest IMR18650	Samsung 30T	A123 26650
Pack Voltage	1000	1000	1000	1000
Nominal Voltage	850	891.7	860.4	
Pack Energy [kWh]	59.4	59.4	59.4	59.4
Number of Cells	5664	5061	5736	7228
Cells in Parallel (n_e)	24	21	24	26
Cells in Series (m_e)	236	241	239	278
Weight of cells (kg)	**263.94**	**273.22**	**401.52**	**549.33**
Weight of pack (kg) Includes 10% to 30% overhead	**290.33 - 343.12**	**300.50 – 355.18**	**441.67 - 521.98**	**604.26 - 714.12**
Specific Energy (Wh/kg)	225.05	217.41	141.45	108.13
Specific Power (W/kg)	2736	3335.54	2100	5685.32

Table 5. 6 Battery pack sizing

The lightest battery pack can be built with the SONY VTC-6, and it also surpasses the specific power and energy requirements of the FE power profile; hence it is the recommended choice of the cell for the FE power profile. Heat generation analysis is performed on the SONY VTC-6 zero-order cell model to estimate the performance of the cell at the pack level.

Formula E	Vehicle Parameters	Estimated Parameters
Nominal voltage (V)	≈878	850
Battery pack weight (kg)	≈280	290.33 - 343.12
Specific energy (Wh/kg)	≈193	225.05
Specific power (W/kg)	≈893*	2736**

* Calculated by dividing the maximum power applied by the vehicles by the battery pack weight
** Calculated by dividing the maximum estimated power output of the battery pack by the estimated total weight of cells

Table 5. 7 Comparing the known vehicle parameters and the estimated parameters

Table 5. 7 provides satisfactory proof of the methodology's competency as the estimated vehicle parameters as relatively close to the known vehicle parameters except for specific power, which is calculated differently for both columns. The battery pack designed using the SONY VTC-6 should be capable of completing the FE race while delivering the required power output.

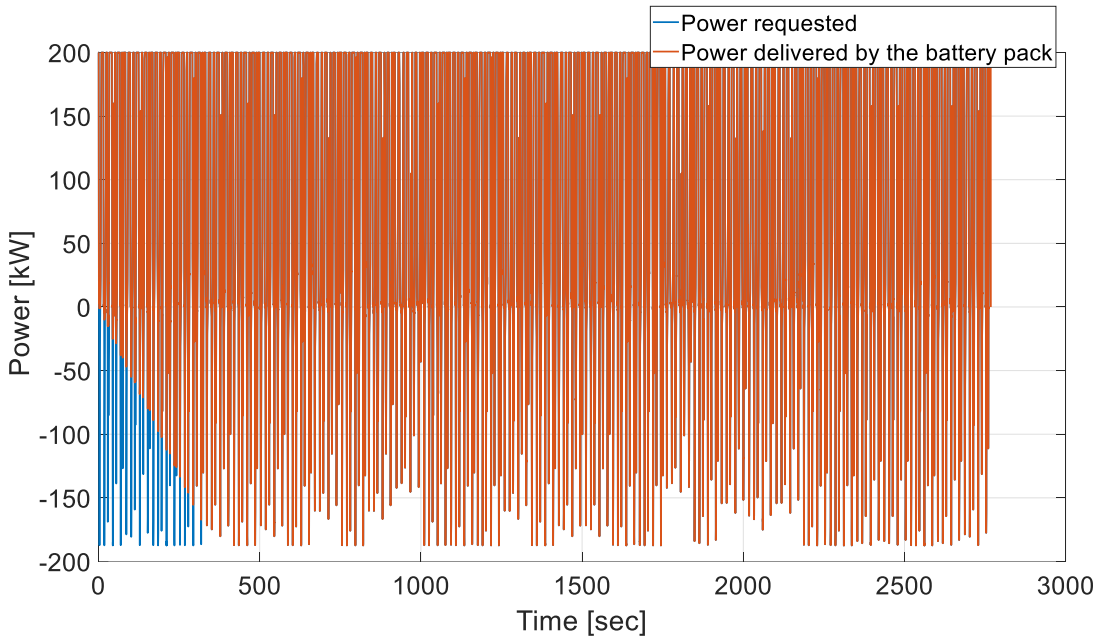

Figure 5. 10 Comparing requested power and delivered power

The FE car is allowed to use 54kWh of the battery pack energy over the duration of the race, but the battery pack needs to be bigger than 54kWh as the terminal voltage of the cells drops below the minimum cell voltage around 2500 seconds, and the battery pack is not capable of delivering power, as estimated by the zero-order battery model. A minimum of 59.4kWh is required to complete the race while delivering and recuperating the requested power. The battery pack hits the power limit during the initial 400 seconds as the battery pack is at 100% SOC and cannot accept any more energy from the electric machine in power regeneration.

The battery pack's operating voltage range is between 1000V and 590V with a maximum discharge current of 720A and a maximum charge current of 576A. During the FE race simulation, the battery pack goes from 100% SOC to 3% SOC, and the voltage drops from 986V to 726V while generating 1609.2kJ of heat. The simulated battery pack behavior is visualized in Figure 5. 11 and Figure 5. 11.

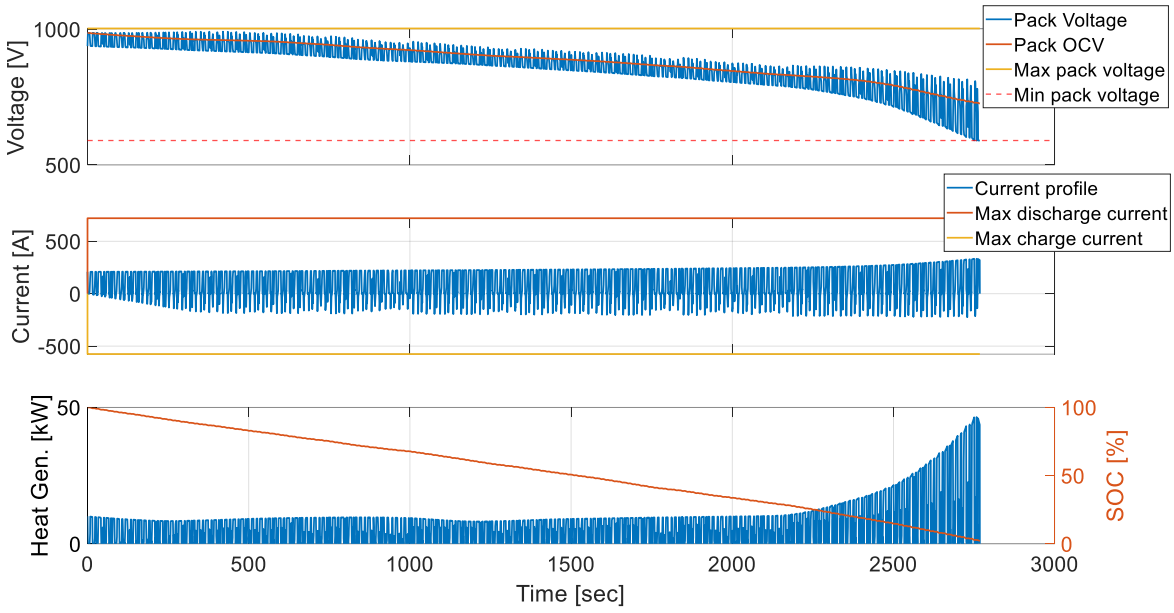

Figure 5. 11 Behavior of battery pack during FE duty cycle

5.4 Cell selection criteria for other motorsports categories:

The generalized methodology is applied to all the race power profiles mentioned in the thesis; the results are tabulated in Table 5. 8, Table 5. 9, and Table 5. 10. The max peak C-rate, max peak C-rate duration, and continuous C-rate duration in table 5. 10 are used to select the most optimal chemistries to suffice the race power profile. The C-rate values in table 5. 10 also represent the stark difference between the racing profiles. Open-wheel racing on closed-circuit racing has a shorter max peak duration as compared to land speed racing or even time-trial due to the length of straight-line tarmac constrained by track layout. PPIHC has one of the most prolonged max peak durations due to the longer straight-line tarmac where the driver can accelerate for a longer duration. In land-speed racing, the only motivation is to achieve maximum straight-line speed, and the driver accelerates for a longer period, leading to a longer max peak duration. Land-speed racing

also requires higher power density and rate of discharge capability to put down the highest amount of power limited by traction, leading to the highest C-rate requirements.

Metric	30 hp E-kart	PPIHC	IOMTT	VBB3	VVW
Duration (min)	15.56	11.05	17.37	1.8	1.83
Distance (km)	17.94	20.66	60.68	-	-
Peak Power (kW)	19.95	132.18	166.15	1605	216.92
Mean power (kW)	10.48	35.13	95.56	1008.40	155.76
SD power (kW)	13.78	34.78	52.85	405.85	64.34
Peak Regen Power (kW)	0	0	0	0	0
Mean Regen Power (kW)	0	0	0	0	0
SD Regen Power (kW)	0	0	0	0	0
Total Energy. (kWh)	2.72	6.47	27.67	30.25	4.77

Table 5. 8 Summary of race data

Parameters	30 hp E-kart	PPIHC	IOMTT	VBB3	VVW
Total Peak Duration (s)	565.11	275.70	630.60	73	69
Number of Peaks	263	127	117	2	1
Mean C-rate total	3.54	4.95	3.14	10.5	10.38
Mean peak C-rate	4.59	10.03	4.19	12.93	12.95
Max C-rate | Duration at Max C-rate (s)	6.74 | 7.66	18.61 | 6.50	5.46 | 5.60	16.71 | 19.47	14.46 | 69
Max Duration [s] | C-rate	8.19 | 6.66	7.9 | 15.78	29.40 | 5.44	53.35 | 14.28	69 | 69
Continuous $\boldsymbol{CR_P}$	3.5	5	3.14	10.5	10.38
Peak $\boldsymbol{CR_P}$	6.75	19	5.5	16.71	69

Table 5. 9 Summary of evaluated metrics

Metric	30 hp E-kart	PPIHC	IOMTT	VBB3	VVW
Max Peak CR_P	6.74	18.61	5.46	16.71	14.46
Max Peak CR_P duration	8.19s	7.9s	29.40	19.50	69
Continuous CR_P	3.54	4.95	3.14	10.5	10.38

Table 5. 10 Metrics for Cell selection

Conclusion

The thesis lays out a detailed procedure for designing an optimal battery pack for any racing application, starting with just the regulations of the racing category. The data acquisition is one of the most challenging tasks required for the analysis, albeit one can use a simple race simulation based on the road-load equation to determine the power profile and follow the generalized methodology to select the right cell chemistry.

The efficacy of the generalized methodology is proven in Table 5. 7 as the estimated FE battery pack specifications are better or in the closed proximity of the parameters initially known. The methodology helped in choosing the most appropriate cell chemistry and battery cell as well as predicting the analytical design of the battery pack and heat generation for the duty cycle. From the heat generation analysis and battery weight estimation, one can guesstimate the kind of thermal management system described in the second chapter needed for the duty cycle.

The analysis of power profiles from different motorsports categories also uncovered the basic demands of each racing category. FE, E-kart requires a right balance between specific power and specific energy, as the vehicle is required to achieve relatively high speeds while traversing a substantially greater distance compared to time-trials or land-speed racing. Land speed racing is more dependent on the specific power, and high discharge rates as the vehicle are required to achieve the maximum possible speed in the shortest possible distance by applying the maximum traction limited power. The aperiodic power profile of time-trials can be more demanding than the open-wheel racing as the race-route is not constrained by the limits of the closed racing area; hence the longer straights could lead to high discharge power profiles.

Future work:

The research done could be further improved by integrating more battery chemistries and zero-order battery models of widely available chemistries in the consumer market, as well the heat transfer analysis of various thermal management systems that could be used to alleviate battery temperature to compare and choose the right configuration of the thermal management system [3]. The whole methodology can be combined into a single expansive algorithm that would take the estimated power profile from a race simulator or telemetry data and output the optimal cell chemistry, battery-pack configuration and specification, and thermal management system configuration for a specific racing application, streamlining the battery pack development process.

References

References for chapter 1:

[1] *Bertha Benz.* www.mercedes-benz.com/en/classic/bertha-benz/.

[2] "August 1888: Bertha Benz Takes World's First Long-Distance Trip in an Automobile." *MarsMediaSite*, media.daimler.com/marsMediaSite/en/instance/ko/August-1888-Bertha-Benz-takes-worlds-first-long-distance-trip-in-an-automobile.xhtml?oid=9361401.

[3] "American, European, and International Racing." *Encyclopædia Britannica*, Encyclopædia Britannica, Inc., www.britannica.com/sports/automobile-racing/American-European-and-international-racing.

[4] "A Brief History of Formula One." *ESPN UK*, en.espn.co.uk/f1/motorsport/story/3831.html.

[5] Person. "1898 Riker Electric: A Green-Motoring Pioneer." *Autoweek*, Autoweek, 5 Sept. 2020, www.autoweek.com/a2010366/1898-riker-electric-green-motoring-pioneer/.

[6] "Timeline: History of the Electric Car." *Energy.gov*, www.energy.gov/timeline/timeline-history-electric-car.

[7] Daimler. "Benz Patent Motor Car: The First Automobile (1885–1886)." *Daimler*, www.daimler.com/company/tradition/company-history/1885-1886.html.

[8] McLaren. "History of the F1 Engine." *McLaren Racing*, 5 June 2020, www.mclaren.com/racing/car/history-of-the-f1-engine/.

[9] F1. "Re-Writing the F1 Rulebook - Part 4: 'Cleaner' Cars, KERS and the Return of Slicks." *Formula 1*, Formula 1, 4 Feb. 2019, www.formula1.com/en/latest/article.re-writing-the-f1-rulebook-part-4-cleaner-cars-kers-and-return-of-slicks.1NUrjfG83a6aE0QSuAkGK8.html.

[10] "Chasing 400." *Center for Automotive Research*, car.osu.edu/news/2017/09/chasing-400.

[11] Holder, Bill. "Formula Lightning Cars - It's Electric! - The Series." *Hot Rod*, Hot Rod, 14 June 2016, www.hotrod.com/articles/ctrp-0204-formula-lightning-cars/.

[12] Matsuda, Emi. "OSU Race Team Wins Cleveland Electric Car Classic." *The Lantern*, 2 Aug. 1998, www.thelantern.com/1998/08/osu-race-team-wins-cleveland-electric-car-classic/.

[13] F1. “Mercedes to Debut Formula 1 MGU-H Technology in AMG Road Cars: Formula 1®.” *Formula 1*, Formula 1, 17 June 2020, www.formula1.com/en/latest/article.mercedes-to-debut-formula-1-mgu-h-technology-in-amg-road-cars.6ha9y57tg2aY33xZsWQjwH.html.

[14] “FIA Formula E.” *History | FIA Formula E*, www.fiaformulae.com/en/discover/history.

[15] Hertzke, Patrick. “Expanding Electric-Vehicle Adoption despite Early Growing Pains.” *McKinsey & Company*, McKinsey & Company, 26 Aug. 2019, www.mckinsey.com/industries/automotive-and-assembly/our-insights/expanding-electric-vehicle-adoption-despite-early-growing-pains.

[16] “ID.R.” *Volkswagen Newsroom*, www.volkswagen-newsroom.com/en/idr-3905.

[17] Berk, Brett. “How Formula E Racing Makes Electric Cars Faster, Smarter, Funner.” *Wired*, Conde Nast, www.wired.com/story/formula-e-electric-car-tech-transfer/.

[18] Fitzpatrick, Alex. “How Formula E Is Driving Electric Vehicle Development.” *Time*, Time, 10 July 2019, time.com/5622578/formula-e/.

[19] FIA Formula E. (n.d.). Retrieved November 23, 2020, from https://www.fiaformulae.com/en/championship/rules-and-regulations

[20] Rowlandjowett. (2020, September 15). Gen3 Formula E: To Charge or Not to Charge? Retrieved November 23, 2020, from https://canopysimulations.com/2019/12/21/gen3-formula-e-to-charge-or-not-to-charge/

[21] FIA Formula E. (2020, November 20). Retrieved November 23, 2020, from https://www.fiaformulae.com/

[22] Electric and New Energy Championship. (2018, January 10). Retrieved November 23, 2020, from https://www.fia.com/events/electric-and-new-energy-championship/season-2017/electric-and-new-energy-championship

[23] Karting, F. (n.d.). Retrieved November 23, 2020, from https://www.fiakarting.com/page/home

[24] About – Fans. (n.d.). Retrieved November 23, 2020, from https://ppihc.org/about-fans/

[25] (n.d.). Retrieved November 23, 2020, from https://www.iomtt.com/tt-info

[25] D'Arpino, M., Cooke, D., Rizzoni, G., & Tomasso, G. (2016, June). Analysis and performance of the venturi buckeye bullet 3 land-speed record attempts. In *2016 IEEE Transportation Electrification Conference and Expo (ITEC)* (pp. 1-7). IEEE.

[26] Land Speed World Records. (n.d.). Retrieved November 23, 2020, from http://www.fim-live.com/en/sport/sport/world-records-attempts/

References for chapter 2:

[1] "Basic Concepts" *Linden's Handbook of Batteries*, by Kirby W. Beard et al., McGraw-Hill Education, New York, 2019.

[2] Ch 1, Lithium-ion batteries.

[3] Ch 1, Battery Management systems

[4] Saw, Lip Huat, Yonghuang Ye, and Andrew AO Tay. "Integration issues of lithium-ion battery into electric vehicles battery pack." *Journal of Cleaner Production* 113 (2016): 1032-1045.

[5] Amjad, Shaik, S. Neelakrishnan, and R. Rudramoorthy. "Review of design considerations and technological challenges for successful development and deployment of plug-in hybrid electric vehicles." *Renewable and Sustainable Energy Reviews* 14.3 (2010): 1104-1110.

[6] Perner, A., and J. Vetter. "Lithium-ion batteries for hybrid electric vehicles and battery electric vehicles." *Advances in battery technologies for electric vehicles*. Woodhead Publishing, 2015. 173-190.

[7] Handbook of lithium-ion battery pack design _ chemistry, components, types, and terminology

[8] Saw, Lip Huat, Yonghuang Ye, and Andrew AO Tay. "Integration issues of lithium-ion battery into electric vehicles battery pack." *Journal of Cleaner Production* 113 (2016): 1032-1045.

[9] Xia, Guodong, Lei Cao, and Guanglong Bi. "A review on battery thermal management in an electric vehicle application." *Journal of power sources* 367 (2017): 90-105. [4] Wang et al. - 2016 - A critical review of thermal management models and

[10] Chen, Dafen, et al. "Comparison of different cooling methods for lithium-ion battery cells." *Applied Thermal Engineering* 94 (2016): 846-854.

[11] Xia, Guodong, Lei Cao, and Guanglong Bi. "A review on battery thermal management in an electric vehicle application." *Journal of power sources* 367 (2017): 90-105.

[12] Wang, Qian, et al. "A critical review of thermal management models and solutions of lithium-ion batteries for the development of pure electric vehicles." *Renewable and Sustainable Energy Reviews* 64 (2016): 106-128.

References for chapter 5:

[1] D'Arpino, M., Cancian, M., Sergent, A., Canova, M., & Perullo, C. (2019). A simulation tool for battery life prediction of a Turbo-Hybrid-Electric Regional Jet for the NASA ULI Program. In *AIAA Propulsion and Energy 2019 Forum* (p. 4469).

[2] Freudiger, D., D'Arpino, M., & Canova, M. (2019). A generalized equivalent circuit model for design exploration of li-ion battery packs using data analytics. *IFAC-PapersOnLine*, *52*(5), 568-573.

[3] Freudiger, D., D'Arpino, M., & Canova, M. (2020, July). Optimal Energy and Thermal Management of Hybrid Battery Packs Using Convex Optimization. In *2020 American Control Conference (ACC)* (pp. 2238-2243). IEEE.